Shape Memory Alloys — Part II: Modeling of Polycrystals

Dimitris C. Lagoudas
Pavlin B. Entchev
Peter Popov
Department of Aerospace Engineering
Texas A&M University
College Station, TX 77843-3141
USA

Etienne Patoor
Laboratory of Physics and Mechanics of Materials
UMR 7554 CNRS - Metz University
ENSAM 4, rue Augustin Fresnel
57045 Metz
FRANCE

L. Catherine Brinson
Xiujie Gao
Mechanical Engineering Department
Northwestern University
Evanston, IL 60208
USA

October 21, 2004

Abstract

The second part of this two-part paper summarizes work on the micromechanical modeling of polycrystalline Shape Memory Alloys (SMAs). Averaging micromechanics methods based on the self-consistent approximation are used for the modeling of polycrystalline SMA thermomechanical behavior. The predictions of several models are directly compared and correlated with experimental results. Rate independent phenomenological models are then discussed, which are based on characterizing the inelastic fields associated with the phase transformation and transformation induced plasticity by using internal state variables. The resulting evolution equations are integrated using return mapping algorithms. Selected numerical simulations and comparison of the phenomenological models with the micromechanical ones are also presented.

Contents

List of Symbols

T	Temperature
T_0	Reference temperature
M_s	Martensitic start temperature (at zero stress level)
M_f	Martensitic finish temperature (at zero stress level)
A_s	Austenitic start temperature (at zero stress level)
A_f	Austenitic finish temperature (at zero stress level)
$\langle\boldsymbol{\sigma}\rangle$, $\boldsymbol{\sigma}$	Macroscopic Cauchy stress tensor
$\langle\boldsymbol{\varepsilon}\rangle$, $\boldsymbol{\varepsilon}$	Linearized, macroscopic, total strain
$\boldsymbol{\varepsilon}^t$	Macroscopic transformation strain
$\boldsymbol{\mathcal{L}}$	Tangent stiffness for a strain increment
$\boldsymbol{\Theta}$	Tangent thermal modulii for a strain increment
$\boldsymbol{\mathcal{L}}^0$	Homogeneous tangent stiffness
$\boldsymbol{\Theta}^0$	Homogeneous tangent thermal modulii
$\boldsymbol{\mathcal{L}}^{\text{eff}}$	Effective tangent stiffness
$\boldsymbol{\Theta}^{\text{eff}}$	Effective tangent thermal modulii
$\mathbf{A}(\mathbf{x})$	Stress concentration (localization) tensor
$\mathbf{a}(\mathbf{x})$	Thermal concentration (localization) tensor
H	Maximum uniaxial transformation strain
I_1	First stress invariant
J_2	Second deviatoric stress invariant
J_3	Third deviatoric stress invariant
G	Gibbs free energy
G^M	Gibbs free energy of the martensitic phase
G^A	Gibbs free energy of the austenitic phase
G^{mix}	Gibbs free energy of the austenite-martensite mixture
ξ	Total volume fraction of martensite (phenomenological)
ξ^t	Volume fraction of twinned martensite (phenomenological)
ξ^d	Volume fraction of detwinned martensite (phenomenological)
ζ^d	Internal variable for transformation induced plasticity
π	Thermodynamic driving force conjugate to ξ
$\boldsymbol{\Lambda}$	Transformation direction tensor
$\boldsymbol{\Lambda}^p$	Plastic direction tensor
$\boldsymbol{\mathcal{S}}^A$	4-th order elastic compliance tensor of austenite
$\bar{\boldsymbol{\alpha}}^A$	2-nd order thermal dilatations tensor of austenite
c^A	specific heat of austenite
s_0^A	specific entropy at the reference state of austenite
u_0^A	internal energy at the reference state of austenite
$\boldsymbol{\mathcal{S}}^M$	4-th order elastic compliance tensor of martensite
$\bar{\boldsymbol{\alpha}}^M$	2-nd order thermal dilatations tensor of martensite
c^M	specific heat of martensite
s_0^M	specific entropy at the reference state of martensite
u_0^M	internal energy at the reference state of martensite
$\boldsymbol{\mathcal{S}}(\xi)$	Effective 4-th order elastic compliance tensor
$\bar{\boldsymbol{\alpha}}(\xi)$	Effective 2-nd order thermal dilatations tensor
$c(\xi)$	Effective specific heat
$s_0(\xi)$	Effective specific entropy at the reference state
$u_0(\xi)$	Effective internal energy at the reference state

1 Introduction

Part I of this review paper focused on the modeling of single crystal SMAs, presenting the kinematics of the martensitic phase transformation and addressing different approaches for the development of the free energy and dissipation in order to formulate thermomechanical constitutive equations. In this Part II results from modeling of polycrystalline SMAs considering both micromechanical approaches and phenomenological ones are presented. This part also includes considerations of the numerical integration of rate-independent SMA constitutive models into finite element codes.

During the last two decades the area of constitutive modeling of *polycrystalline* SMAs has been a topic of many research publications and significant advancements have been reported. The majority of the constitutive models reported in the literature can be formally classified to belong to one of the two groups: micromechanics-based models and phenomenological models. Recently Roubiček (2004) reviewed these two types of models as well as atomistic-level simulations of shape memory behavior.

The micromechanical models attempt to predict the SMA response by taking into account the granular microstructure of polycrystalline SMAs. Theoretically, if the micro-structure is well-known it is possible to use the well developed knowledge of single crystal SMA behavior and solve boundary value problems in a polycrystalline material. Anand and Gurtin (2003) for example, use a model for single crystal SMA and perform representative numerical calculations for the response of polycrystals with random orientation of the single crystals. In practice, however one neither has exact representation of the micro-structure, nor is it possible to solve numerically problems involving sufficient number of grains, as would happen in realistic, three-dimensional boundary value problems. It is therefore necessary to use homogenization techniques in order to obtain representative thermomechanical properties of a polycrystalline material.

These type of problems first arose in the context of homogenizing the macroscopic properties of heterogeneous composite materials. Many homogenization methods have been developed over the years for elastic and elastoplastic materials, among which averaging methods (Hershey, 1954; Kröner, 1958; Hill, 1965; Mori

and Tanaka, 1973; Christensen, 1991; Nemat-Nasser and Hori, 1993) which typically consider ellipsoid inclusion in a Representative Volume Element (RVE) and asymptotic expansion methods, initially developed for periodic microstructure (Bensoussan et al., 1978; Sanchez-Palencia, 1980; Bakhvalov and Panasenko, 1990; Zhikov et al., 1994; Gaymonat et al., 1993).

Most of the micromechanical models for polycrystalline SMAs are based on a self consistent type of averaging methods (Patoor et al., 1987; Falk, 1990; Patoor et al., 1996; Lagoudas and Bhattacharya, 1997; Lu and Weng, 1998; Gao and Brinson, 2002). Such an approach was developed for the elastoplastic behavior of heterogeneous materials by Berveiller et al. (1994). In the present work two micromechanical models for polycrystalline SMAs - the one developed by Patoor et al. (1996) and by Gao and Brinson (2002) are presented and compared.

The other class of models for polycrystalline SMAs are phenomenological ones which rely on continuum thermomechanics with internal variables to account for the changes in the microstructure due to phase transformation. These type of models usually assume a macroscopic energy function that depends on state and internal variables used to describe the degree of phase transformation. Evolution equations are then postulated for the internal variables. The macroscopic energy and the evolution equations are assumed to have a certain functional form, which must be compatible with thermodynamics. The fundamental structure of all these models is very similar, and can be classified as that of constitutive models with internal state variables (Hill, 1967; Kestin and Rice, 1970; Rice, 1971; Kestin and Bataille, 1977). The resulting phenomenological models do not directly depend on material parameters at the microscopic level, but on a set of parameters at the macroscopic level which are determined by experimental observations. Such models can be very simple, for example modeling the uniaxial pseudoelastic response of an SMA by a piecewise linear function, or can be very complex, as in 3-D models, involving a number of material parameters which have to be determined by extensive experimentation and often do not have obvious physical interpretation. Phenomenological models are easily implementable in numerical methods for the solution of boundary value problems on the structural (macroscopic) level, and, depending on the application, one has the flexibility to make numerous trade-offs between accuracy and complexity. An alternative to using internal variables and defining evolution equations, as in classical plasticity, are the energy minimization methods. In one of the early examples, Ball and James (1987) modeled the SMA as a nonlinear elastic material and postulated a two-well free energy function. By determining energy minimizing deformations with two coherent and macroscopically unstressed variants of martensite it is possible to find a microstructure which corresponds to the loading conditions. Energy minimization methods will not be discussed in this paper.

Significant effort has been devoted over the past decade to establish phenomenological constitutive models describing the macroscopic thermomechanical response of polycrystalline SMAs (Tanaka, 1986; Sato and Tanaka, 1988; Tanaka et al., 1992, 1995; Patoor et al., 1987, 1988; Ortin and Planes, 1988, 1989; Berveiller et al., 1991; Liang and Rogers, 1990, 1992; Sun et al., 1991; Sun and Hwang, 1993a,b; Graesser and Cozzarelli, 1991; Brinson, 1993; Raniecki and Lexcellent, 1994; Boyd and Lagoudas, 1994b, 1996a,b; Lagoudas et al., 1994, 1996; Marketz and Fischer, 1995; Marketz et al., 1995; Bekker and Brinson, 1997, 1998; Leclercq and Lexcellent, 1996; Lagoudas and Shu, 1999; Juhasz et al., 2002; Bo and Lagoudas, 1999a,b,c; Lagoudas and Bo, 1999; Lexcellent et al., 2000; Lagoudas and Entchev, 2004). Most of the constitutive models adopt a thermodynamic structure and select the martensitic volume fraction as an internal state variable to account, on the average, for the influence of the microstructure.

The early constitutive models (Tanaka, 1986; Tanaka et al., 1986, 1995; Liang and Rogers, 1990, 1992; Brinson, 1993; Boyd and Lagoudas, 1994a, 1996a) have been used to derive the pseudoelastic response of SMAs and their main difference is the hardening function selected to model the stress-strain response during the stress induced martensitic phase transformation. A unified framework for these early constitutive models has been presented by Lagoudas et al. (1996). Further improvements in the accuracy of SMAs models was achieved by Raniecki and Lexcellent (1998); Qidwai and Lagoudas (2000b); Lexcellent et al. (2002), who proposed different transformation functions in order to capture the asymmetric response that SMAs exhibit in tension and compression. Qidwai and Lagoudas (2000b) also studied the consequences the principle of maximum dissipation during phase transformation has on the transformation surface and flow rules. The one-dimensional model of Brinson (1993) was one of the first to include modeling of detwinning of martensite. The work was based on a phase diagram approach and used two volume fractions of martensite to model pseudoelasticity and detwinning separately. It was further refined by Bekker and Brinson (1997, 1998). A thermodynamics based model of detwinning has been proposed by Leclercq and Lexcellent (1996); Lagoudas and Shu (1999); Juhasz et al. (2002). Reorientation of martensite during non-proportional loading has been taken into account by Boyd and Lagoudas (1994a), who used a non-associative flow rule during the reverse transformation. Juhasz et al. (2002) addressed this issue by using both the martensitic volume fraction

and the transformation strain as separate internal variables. Cyclic loading and transformation induced plasticity in SMAs has also been a major research topic in SMA modeling (Tanaka et al., 1995; Lexcellent and Bourbon, 1996; Bo and Lagoudas, 1999a,b,c; Lagoudas and Bo, 1999; Lexcellent et al., 2000; Lagoudas and Entchev, 2004). In the works of Tanaka et al. (1995); Lexcellent and Bourbon (1996) it is assumed that a portion of the martensite does not recover after each cycle, which leads to observable unrecoverable strain, which eventually saturates with the number of cycles. In the one dimensional model of Bo and Lagoudas (1999a,b,c) and Lagoudas and Bo (1999) the stress-induced transformation is modelled by allowing both transformation and plastic strains to develop simultaneously as a result of the applied load. The work was later extended by Lagoudas and Entchev (2004) to three dimensions.

The models reviewed above are rate independent ones, having a stress-strain response dependant only on the loading path. Rate dependent constitutive models have also been proposed in the literature. An early example is the model by Achenbach (1989), who uses two-well potentials for the free energy and statistical physics to justify transition probabilities between two different variants of martensite (one in tension and one in compression) and austenite. The formulation of the model allows for a softening stress-strain relationship. In a recent paper this model is extended my Govindjee and Hall (2000), who used multi-well potentials and an arbitrary number of martensitic variants. Other authors have directly coupled a nonlinear thermoelastic potential and a kinetic relation to solve wave propagation problems in one-dimensional SMA rods. Abeyaratne and Knowles (1994a,b, 1997) have solved the Riemann problem in both isothermal and adiabatic settings for an SMA with softening behavior. A kinetic relation defining the speed of propagation of the phase front is introduced as a constitutive relation in order to enforce uniqueness of the Riemann problem.

The numerical implementation of phenomenological models has also been an active area of research (Auricchio et al., 1997; Auricchio, 2001; Qidwai and Lagoudas, 2000a; Govindjee and Miehe, 2001). While the computational methods have their roots in algorithms used in computational plasticity (cf. Ortiz and Popov (1985); Simo and Hughes (1998)), the complex behavior of SMAs requires the development of specialized algorithms.

This second part of the paper is organized as follows: in Section 2, the self-consistent approach used in micromechanical modeling of SMAs is presented and the models by Patoor et al. (1996) and by Gao and Brinson (2002) are reviewed and compared. In Section 3 an attempt is made to review and classify some of the huge number of phenomenological models that have been published in the literature. The paper is concluded in Section 4 with a typical numerical implementation of a phenomenological model.

2 Micromechanical Modeling of Polycrystalline SMA Behavior

2.1 Thermomechanical Integral Equation

In Part I of the current paper constitutive relations were determined for single crystals, where the crystallographical orientation is completely defined and where mechanical loading conditions are considered to be uniform on the whole volume. Such an accurate analysis is impossible in polycrystalline materials. Existence of the granular structure leads to strain incompatibilities. This phenomenon produces an intergranular stress field. A priori knowledge of the local loading conditions on each grain is impossible, so the use micromechanical averaging methods must considered.

Three fundamental equations govern the scale transition problem. The first is the stress equilibrium condition. Given the inelastic character of the behavior, this condition is expressed in rate form (cf. e.g. Malvern (1969)):

$$\mathrm{div}\dot{\boldsymbol{\sigma}} = 0. \tag{2.1}$$

The second fundamental equation is the compatibility condition of the total strain field. Local quantities must satisfy the imposed boundary conditions. Consider a velocity field $\mathbf{v}(\mathbf{x})$ applied on the surface ∂V of the RVE:

$$\mathbf{v} = \dot{\mathbf{u}} = \langle\dot{\boldsymbol{\varepsilon}}\rangle\mathbf{x} \quad \text{for} \quad \mathbf{x} \in \partial V, \tag{2.2}$$

where $\langle\dot{\boldsymbol{\varepsilon}}\rangle$ is the average strain increment, defined over the volume V of the RVE. As in the first part the notation $\langle\cdot\rangle$ is used to denote averaging over the RVE.

The linearized strain rate tensor is given by

$$\dot{\boldsymbol{\varepsilon}} = \frac{1}{2}(\nabla\dot{\mathbf{u}} + (\nabla\dot{\mathbf{u}})^{\mathrm{T}}). \tag{2.3}$$

This equation ensures strain field compatibility in the solid. The local constitutive law, is the third relationship, which in incremental forms reads:

$$\dot{\boldsymbol{\sigma}} = \boldsymbol{\mathcal{L}}\dot{\boldsymbol{\varepsilon}} - \boldsymbol{\Theta}\dot{T}. \tag{2.4}$$

The linearized strain rate $\dot{\boldsymbol{\varepsilon}}$ is composed of a thermoelastic part and an inelastic part that is directly linked to the phase transformation. Introducing the local behavior (2.4) in the equilibrium condition (2.1) gives

$$\operatorname{div}\left(\boldsymbol{\mathcal{L}}\dot{\boldsymbol{\varepsilon}} - \boldsymbol{\Theta}\dot{T}\right) = 0. \tag{2.5}$$

Consider a homogenized reference medium characterized by two homogeneous tangent modulii $\boldsymbol{\mathcal{L}}^0$ and $\boldsymbol{\Theta}^0$. A uniform strain rate $\boldsymbol{\varepsilon}^0$ is applied to this medium. The tangent modulii in the constitutive law (2.4) are defined by their spatial deviations $\delta\boldsymbol{\mathcal{L}}$ and $\delta\boldsymbol{\Theta}$ from these homogeneous quantities:

$$\boldsymbol{\mathcal{L}} = \boldsymbol{\mathcal{L}}^0 + \delta\boldsymbol{\mathcal{L}} \tag{2.6a}$$

$$\boldsymbol{\Theta} = \boldsymbol{\Theta}^0 + \delta\boldsymbol{\Theta}. \tag{2.6b}$$

Substituting the last two relations in the equilibrium equation (2.5) gives:

$$\operatorname{div}\left(\left(\boldsymbol{\mathcal{L}}^0 + \delta\boldsymbol{\mathcal{L}}\right)\dot{\boldsymbol{\varepsilon}} - \left(\boldsymbol{\Theta}^0 + \delta\boldsymbol{\Theta}\right)\dot{T}\right) = 0. \tag{2.7}$$

For simplicity, it is assumed that the temperature field is homogeneous and equal to the imposed test temperature. This implies that $\operatorname{div}(\boldsymbol{\Theta}^0\dot{T}) = 0$, so the last equation becomes:

$$\operatorname{div}\left(\boldsymbol{\mathcal{L}}^0(\nabla\dot{\mathbf{u}})\right) + \operatorname{div}\left(\delta\boldsymbol{\mathcal{L}}\dot{\boldsymbol{\varepsilon}} - \delta\boldsymbol{\Theta}\dot{T}\right) = 0. \tag{2.8}$$

The second part of this equation can be considered the time-derivative of a volume force $\mathbf{f}(\mathbf{x})$ such that, for each point $\mathbf{x}$,

$$\operatorname{div}\left(\boldsymbol{\mathcal{L}}^0(\nabla\dot{\mathbf{u}})\right) + \dot{\mathbf{f}} = 0, \tag{2.9}$$

where

$$\dot{\mathbf{f}} = \operatorname{div}\left(\delta\boldsymbol{\mathcal{L}}\dot{\boldsymbol{\varepsilon}} - \delta\boldsymbol{\Theta}\dot{T}\right). \tag{2.10}$$

The Green's function $\mathbf{G}^0$ of an infinite homogeneous reference medium is defined by

$$\boldsymbol{\mathcal{L}}^0\nabla(\nabla\mathbf{G}^0(\mathbf{x}-\mathbf{x}')) + \mathbf{I}\delta(\mathbf{x}-\mathbf{x}') = 0, \tag{2.11}$$

where $\delta(\mathbf{x}-\mathbf{x}')$ is the Dirac function. Setting

$$\dot{\mathbf{u}}(\mathbf{x}) = \int_V \delta(\mathbf{x}-\mathbf{x}')\dot{\mathbf{u}}(\mathbf{x}')dV', \tag{2.12}$$

the following integral equation is obtained from equation (2.11):

$$\dot{\mathbf{u}}(\mathbf{x}) = \dot{\mathbf{u}}^0 + \int_V \mathbf{G}(\mathbf{x}-\mathbf{x}')\dot{\mathbf{f}}(\mathbf{x}')dV', \tag{2.13}$$

where $\dot{\mathbf{u}}^0$ is the solution for a homogeneous reference medium, subject to the same boundary conditions. Substituting equation (2.13) into equation (2.3) leads to the following integral equation in term of strain rate:

$$\dot{\boldsymbol{\varepsilon}}(\mathbf{x}) = \boldsymbol{\varepsilon}^0 + \int_V \boldsymbol{\Gamma}^0(\mathbf{x}-\mathbf{x}')\left(\delta\boldsymbol{\mathcal{L}}(\mathbf{x}')\dot{\boldsymbol{\varepsilon}}(\mathbf{x}') - \delta\boldsymbol{\Theta}(\mathbf{x}')\dot{T}\right)dV', \tag{2.14}$$

where $\boldsymbol{\Gamma}^0$ is the symmetrical part of the modified Green's function.

The solution of this last integral equation theoretically determines the macroscopic behavior. However, this is not trivial. Considering a particular microstructure leads to an approximation of equation (2.14). The classical paper by Hill (1965), for example, considers linear elastic grains in a serial arrangement in the polycrystal. Such microstructure leads to the homogeneity of the stress field. The same microstructure has been used later by Zaoui (1985) to homogenize plastic materials. This kind of simplified approach has been applied to describe pseudoelasticity in SMAs by Patoor et al. (1992). Using a parallel grain

distribution on the other hand leads to uniformity of the strain field and defines the Taylor model. These two types of solutions possess an extremal character and constitute upper and lower bounds for the real behavior. However, the static model underestimates the influence of the internal stress field and the Taylor model greatly overestimates it. The hypothesis of a fully disordered material also simplifies the solution of equation (2.14), while preserving a correct estimation of the internal stress field. This last approach defining the self-consistent models was developed for the elastoplastic behavior of microheterogeneous materials by Berveiller et al. (1994). In the next section, this kind of approach is extended to the case of pseudoelastic Cu-based alloys.

2.2 Self-Consistent Approximation

The integral equation (2.14) is solved using the self-consistent approximation. In this scheme, particular properties of the modified Green's function are used. This tensor can be decomposed into a local part $\mathbf{\Gamma}^{0l}$ and a non-local part $\mathbf{\Gamma}^{nl}$ (Dederichs and Zeller, 1973), which is rapidly decreasing:

$$\mathbf{\Gamma}^0(\mathbf{x}-\mathbf{x}') = \mathbf{\Gamma}^{0l}(\mathbf{x})\delta(\mathbf{x}-\mathbf{x}') + \mathbf{\Gamma}^{nl}(\mathbf{x}-\mathbf{x}'). \tag{2.15}$$

The decomposition (2.15) transforms equation (2.14) into

$$\begin{aligned} \dot{\boldsymbol{\varepsilon}}(\mathbf{x}) &= \boldsymbol{\varepsilon}^0 + \mathbf{\Gamma}^{0l}\left(\delta\boldsymbol{\mathcal{L}}(\mathbf{x})\dot{\boldsymbol{\varepsilon}}(\mathbf{x}) - \delta\boldsymbol{\Theta}(\mathbf{x})\dot{T}\right) \\ &+ \int_V \mathbf{\Gamma}^{nl}(\mathbf{x}-\mathbf{x}')\left(\delta\boldsymbol{\mathcal{L}}(\mathbf{x}')\dot{\boldsymbol{\varepsilon}}(\mathbf{x}') - \delta\boldsymbol{\Theta}(\mathbf{x}')\dot{T}\right)dV' \end{aligned} \tag{2.16}$$

All the difficulties linked to the solution of this equation come from the last term. This problem can be simplified by selecting a homogeneous reference medium, for which the nonlocal term in equation (2.16) is neglected. The later is equivalent to the non-local term $\boldsymbol{\mathcal{L}}\dot{\boldsymbol{\varepsilon}} - \delta\boldsymbol{\Theta}\dot{T}$ in equation (2.8) having a zero mean in the RVE, that is,

$$\int_V \left(\delta\boldsymbol{\mathcal{L}}\dot{\boldsymbol{\varepsilon}} - \delta\boldsymbol{\Theta}\dot{T}\right)dV = 0. \tag{2.17}$$

With the help of (2.6a) and (2.6b) this implies that

$$\int_V \left(\boldsymbol{\mathcal{L}}\dot{\boldsymbol{\varepsilon}} - \boldsymbol{\Theta}\dot{T}\right)dV - \int_V \boldsymbol{\mathcal{L}}^0\dot{\boldsymbol{\varepsilon}}dV + \boldsymbol{\Theta}^0\dot{T} = 0, \tag{2.18}$$

which is equivalent to

$$\langle\dot{\boldsymbol{\sigma}}\rangle = \boldsymbol{\mathcal{L}}^0\langle\dot{\boldsymbol{\varepsilon}}\rangle - \boldsymbol{\Theta}^0\dot{T}. \tag{2.19}$$

So, the particular choice (2.17) is equivalent to choosing as the homogeneous reference medium be the effective medium i.e.,

$$\boldsymbol{\mathcal{L}}^0 = \boldsymbol{\mathcal{L}}^{\text{eff}} \tag{2.20a}$$

$$\boldsymbol{\Theta}^0 = \boldsymbol{\Theta}^{\text{eff}}. \tag{2.20b}$$

This assumption greatly simplifies the solution of the integral equation (2.16), which now turns into

$$\begin{aligned} \dot{\boldsymbol{\varepsilon}}(\mathbf{x}) &= \boldsymbol{\varepsilon}^0 + \mathbf{\Gamma}^{\text{eff}}\left(\boldsymbol{\mathcal{L}}(\mathbf{x}) - \boldsymbol{\mathcal{L}}^{\text{eff}}\right)\dot{\boldsymbol{\varepsilon}}(\mathbf{x}) \\ &- \mathbf{\Gamma}^{\text{eff}}\left(\boldsymbol{\Theta}(\mathbf{x}) - \boldsymbol{\Theta}^{\text{eff}}\right)\dot{T} \end{aligned} \tag{2.21}$$

In this way, two localization tensors $\mathbf{A}(\mathbf{x})$ and $\mathbf{a}(\mathbf{x})$ are defined. They connect the local quantity $\dot{\boldsymbol{\varepsilon}}(\mathbf{x})$ to the global quantities $\boldsymbol{\varepsilon}^0$ and $\dot{T}$ in such a way that equation (2.21) is now expressed as

$$\dot{\boldsymbol{\varepsilon}}(\mathbf{x}) = \mathbf{A}(\mathbf{x})\langle\dot{\boldsymbol{\varepsilon}}\rangle - \mathbf{a}(\mathbf{x})\dot{T}. \tag{2.22}$$

These localization tensors $\mathbf{A}(\mathbf{x})$ and $\mathbf{a}(\mathbf{x})$ are defined by:

$$\mathbf{A}(\mathbf{x}) = \left(\mathbf{I}^4 - \mathbf{\Gamma}^{\text{eff}}\left(\boldsymbol{\mathcal{L}}(\mathbf{x}) - \boldsymbol{\mathcal{L}}^{\text{eff}}\right)\right)^{-1} \tag{2.23a}$$

$$\mathbf{a}(\mathbf{x}) = \mathbf{A}(\mathbf{x})\mathbf{\Gamma}^{\text{eff}}\left(\boldsymbol{\Theta}(\mathbf{x}) - \boldsymbol{\Theta}^{\text{eff}}\right). \tag{2.23b}$$

Defining these quantities, the uniform tangent modulii used in equation (2.19) is determined from the constitutive equation (2.4):

$$\boldsymbol{\mathcal{L}}^{\text{eff}} = \frac{1}{V}\int_V \boldsymbol{\mathcal{L}}\mathbf{A}dV, \tag{2.24a}$$

$$\boldsymbol{\Theta}^{\text{eff}} = \frac{1}{V}\int_V (\boldsymbol{\mathcal{L}}\mathbf{a} + \boldsymbol{\Theta})\, dV. \tag{2.24b}$$

Assuming polycrystals to be sets of homogeneous grains allows the localization tensors to be taken as piecewise uniform functions. Denoting the uniform tangent modulii of grain k by $\boldsymbol{\mathcal{L}}^k$ and the constant value of the localization tensor in this grain by $\mathbf{A}^k$, equation (2.24) becomes

$$\boldsymbol{\mathcal{L}}^{\text{eff}} = \sum_{k=1}^{K} \boldsymbol{\mathcal{L}}^k \mathbf{A}^k \vartheta^k, \tag{2.25}$$

where ϑ^k represents the volume fraction of grain k. In the polycrystal, each grain is characterized by its crystallographic orientation (determined from X-ray diffraction), its shape (from the $\boldsymbol{\Gamma}^{0l}$ tensor) and by ϑ^N. The overall behavior is then totally determined using equation (2.25) from the knowledge of the internal structure evolution in the polycrystalline material. Intergranular interactions coming from the crystallographical misorientation are obtained by the calculation of the stress in each grain.

2.3 Numerical Results

A self-consistent code (Lipinski et al., 1990) developed to describe the plastic behavior in polycrystalline metallic alloys has been modified to compute the pseudoelastic behavior of shape memory alloys. Since the macroscopic reversible strain is less than 10%, this code is used for small deformations, and grain rotation is ignored. Variants of martensite replace slip systems, and the volume fractions of these variants are now the microstructural parameters describing the internal state evolution. Physical constraints (equation (I-5.29)) acting on these variables have been introduced. Recovery of the inelastic strain and hysteretic effect on unloading are taken into account. Numerical results obtained are analyzed and compared to experimental observations performed on CuZnAl alloys. Note that some models reviewed here can also predict shape memory effect. In addition, many alloy systems with different compositions have also been simulated. The reader is referred to Gao and Brinson (2002), Gao et al. (2000) and Huang et al. (2000) for more details.

2.3.1 Crystallographic Data

The elastic behavior is assumed to be isotropic and homogeneous in the two phases (μ ∼40GPa and ν ∼0.3). The polycrystalline structure is schematized by one hundred spherical grains that are randomly oriented to produce an isotropic texture. The main crystallographic characteristics of the martensitic transformation for CuZnAl shape memory alloys are the ones reported by De Vos et al. (1978). These characteristics are considered to be invariant during the transformation. Optical microscopy combined with image analysis give access to the shape of the different grains. X-rays measurement provides a representation of the crystallographic texture of the polycrystal. The measurement of the lattice parameters in the two phases and the mutual orientation relationships helps to determine the habit plane normals $\mathbf{n}$, the transformation directions $\mathbf{m}$ and the strain intensity γ, using the WLR phenomenological theory (Wechsler et al., 1953) for the martensitic transformation (Table 1). Uniaxial tensile tests performed on a single crystal at different temperatures were used to estimate the coefficient B needed in equation (I-5.67) (B ∼0.23MPaK^{-1} in the alloys used).

Existence of compatibility (or incompatibility) relationships between variants is taken into account by the interaction matrix H^{mn}. Micromechanical determination using minimization of equation (I-5.82) according to the orientation of the inclusion considered (Patoor et al., 1996) established that this matrix (see Table 2) is composed using two types of terms: weak interaction terms H^1 for self-accommodated variants (around $\mu/1000$) and strong interaction terms H^2 for incompatible variants (about $\mu/150$). Such distinction is in agreement with metallographical observations (Adachi et al., 1988).

$$\left.\begin{array}{l} H^1 \approx \mu/1000 \approx 40\text{MPa} \\ H^2 \approx \mu/150 \approx 270\text{MPa} \end{array}\right\} \quad \text{for CuZnAl alloy.} \tag{2.26}$$

a	n_1	n_2	n_3	m_1	m_2	m_3
b	n_1	n_3	n_2	m_1	m_3	m_2
c	$-n_1$	n_2	n_3	$-m_1$	m_2	m_3
d	$-n_1$	n_3	n_2	$-m_1$	m_3	m_2
e	$-n_2$	n_1	n_3	$-m_2$	m_1	m_3
f	$-n_3$	n_1	n_2	$-m_3$	m_1	m_2
g	$-n_2$	$-n_1$	n_3	$-m_2$	$-m_1$	m_3
h	$-n_3$	$-n_1$	n_2	$-m_3$	$-m_1$	m_2
i	n_1	$-n_2$	n_3	m_1	$-m_2$	m_3
j	n_1	$-n_3$	n_2	m_1	$-m_3$	m_2
k	$-n_1$	$-n_2$	n_3	$-m_1$	$-m_2$	m_3
l	$-n_1$	$-n_3$	n_2	$-m_1$	$-m_3$	m_2

$n_1 = -0.182 \quad n_2 = 0.669 \quad n_3 = 0.721$

m	n_3	n_1	n_2	m_3	m_1	m_2
n	n_2	n_1	n_3	m_2	m_1	m_3
o	n_3	$-n_1$	n_2	m_3	$-m_1$	m_2
p	n_2	$-n_1$	n_3	m_2	$-m_1$	m_3
q	n_2	$-n_3$	$-n_1$	m_2	$-m_3$	$-m_1$
r	n_3	$-n_2$	$-n_1$	m_3	$-m_2$	$-m_1$
s	$-n_2$	n_3	$-n_1$	$-m_2$	m_3	$-m_1$
t	$-n_3$	n_2	$-n_1$	$-m_3$	m_2	$-m_1$
u	$-n_3$	$-n_2$	$-n_1$	$-m_3$	$-m_2$	$-m_1$
v	$-n_2$	$-n_3$	$-n_1$	$-m_2$	$-m_3$	$-m_1$
w	n_3	n_2	$-n_1$	m_3	m_2	$-m_1$
x	n_2	n_3	$-n_1$	m_2	m_3	$-m_1$

$m_1 = -0.165 \quad m_2 = -0.737 \quad m_3 = 0.655$

Table 1: Definition of the normal to the habit plane and the direction of transformation for each martensitic variant in a CuZnAl SMA (De Vos et al., 1978).

	a	b	c	d	e	f	g	h	i	j	k	l	m	n	o	p	q	r	s	t	u	v	w	x
a	C	C	C	C			C		C		C			C						C	C			
b	C	C	C	C				C		C		C	C						C			C		
c	C	C	C	C	C				C		C					C		C					C	
d	C	C	C	C		C				C		C			C		C							C
e			C		C	C	C	C	C					C		C	C					C		
f				C	C	C	C	C		C			C		C			C			C			
g	C				C	C	C	C			C			C		C			C					C
h		C			C	C	C	C				C	C		C					C			C	
i	C		C		C				C	C	C	C				C				C	C			
j		C		C		C			C	C	C	C			C				C			C		
k	C		C				C		C	C	C	C		C				C					C	
l		C		C				C	C	C	C	C	C				C							C
m		C				C		C				C	C	C	C	C		C				C		
n	C				C		C				C		C	C	C	C	C					C		
o				C		C		C		C			C	C	C	C				C			C	
p			C		C		C		C				C	C	C	C			C					C
q				C	C							C		C			C	C	C	C		C		C
r			C			C					C		C				C	C	C	C	C		C	
s		C					C			C						C	C	C	C	C		C		C
t	C							C	C						C		C	C	C	C	C		C	
u	C					C			C				C					C		C	C	C	C	C
v		C			C					C				C			C		C		C	C	C	C
w			C					C			C				C			C		C	C	C	C	C
x				C			C					C				C	C		C		C	C	C	C

Table 2: Interaction Matrix H^{mn} Determined for CuZnAl Shape Memory Alloy: C Denotes the Compatible Interactions (H^1) and Blank Denotes the Incompatible Ones (H^2) (Patoor et al., 1994).

Note that none of the other models discussed in this paper have considered compatibility or incompatibility in this way since either only one variant is considered or interaction among variants has been considered through their driving forces.

The hysteresis phenomenon linked to the transformation is related to the critical force F_c. Measurement of temperatures M^s and A^f allows the evaluation of the amplitude of this force using equation (I-5.68):

$$2F_c = B(A^f - M^s). \tag{2.27}$$

Temperatures A^f and M^s depend on the material composition. The difference between these two temperatures is almost constant for a given class of alloys but is very sensitive to the thermomechanical loading history. This aspect is not studied here; F_c is considered as being constant along the loading path. It is worthwhile to note that the different material parameters used in this work are measurable quantities, except for H^1 and H^2 used in Patoor et al. (1996), which are determined from micromechanical considerations. There is no use of adjustable parameters in this approach.

2.3.2 Numerical Results

In this section all simulation results are predicted by the model of Patoor et al. (1996) except as mentioned explicitly. For figures showing only the simulations of Patoor et al. (1996), the results by Gao and Brinson (2002) are quite similar and are omitted for clarity.

From these data, the polycrystalline behavior is determined for a given thermomechanical loading path. Figure 1 illustrates results obtained for a uniaxial tensile test at room temperature (T=20°C) using the

model of Patoor et al. (1996) while figure 2 shows the results obtained by Gao and Brinson (2002). In this example, the temperatures M^s and A^f are equal to 10°C and 15°C, respectively. Several characteristics obtained are in agreement with experimental observations:

- the maximum transformation strain is close to 3%, which is realistic for copper-based alloys;
- the hysteresis size determined at the polycrystalline level (45 MPa) is greater than the one for the monocrystalline case used in the constitutive equation (10 MPa);
- the critical transformation stress is in agreement with the well-known Patel and Cohen (1953) relationship.

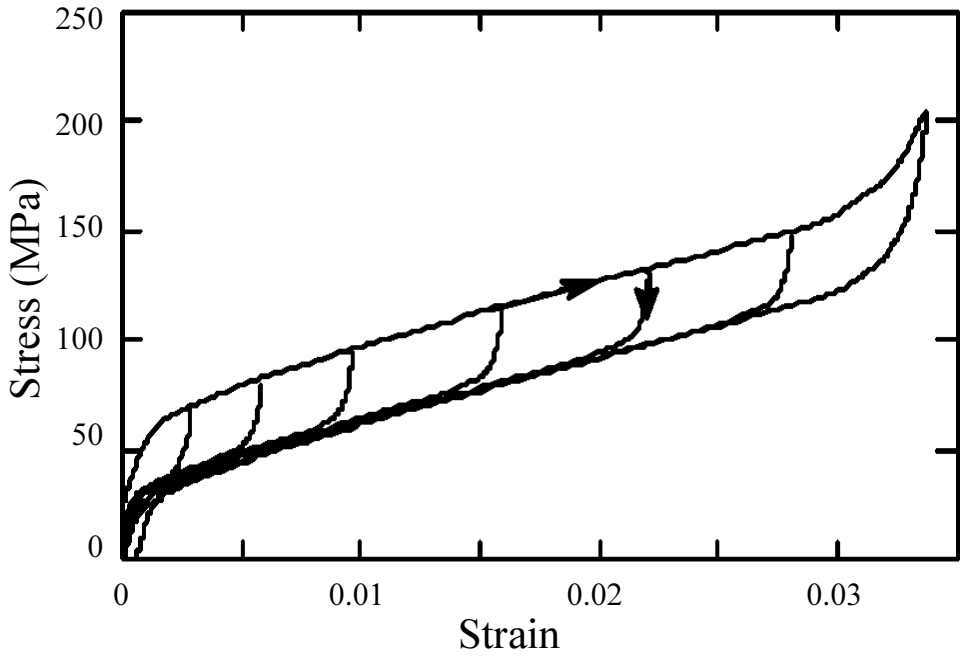

Figure 1: Numerical simulation obtained using the self-consistent approach for tensile test on a polycrystalline pseudoelastic CuZnAl alloy. Computation performed at room temperature ($T = 20$°C), $A^f = 15$°C. The simulation is performed using the model by Patoor et al. (1996).

In these simulations, several stages may be distinguished in the course of the transformation. At the very beginning, the macroscopic transformation strain is very weak. Around 60 MPa, a sharp variation is observed on the stress-strain curve, which defines an apparent macroscopic critical transformation stress. The transformation then proceeds in a steady-state regime. In this second regime, the hardening rate of the simulation in (Patoor et al., 1996) given by the ratio $d\langle\boldsymbol{\sigma}\rangle/d\langle\boldsymbol{\varepsilon}^t\rangle$ is close to 3500 MPa. However, apparent hardening in experiments is often due to local heating through latent heat generation during phase transformation. The rate of hardening is therefore dependent on the strain rate and surrounding heat transfer (Brinson et al., 2002a,b). Gao and Brinson (2002) can capture hardening due to this mechanism when solved in conjunction with heat transfer equations to provide the temperature profile. The simulation here is performed isothermally and therefore lacks the hardening characteristic, but otherwise is quite similar to the simulation in (Patoor et al., 1996).

Evolutions of the internal variables involved in the macroscopic two-phase approach developed in Section 3 are computed. Numerical determination of the evolution of the global martensitic volume fraction f according to the loading defines the kinetic for the stress-induced transformation (Figure 3). A quasi-linear relationship is observed during the steady-state regime of Figure 3. A saturation value around 80% of stress-induced martensite is observed. The end of the transformation is associated with a very large stress without physical meaning. In these conditions, it is no longer possible to assume that the transformation mechanism occurs alone; other physical phenomena must appear (plasticity, crack initiation), and the transformation should

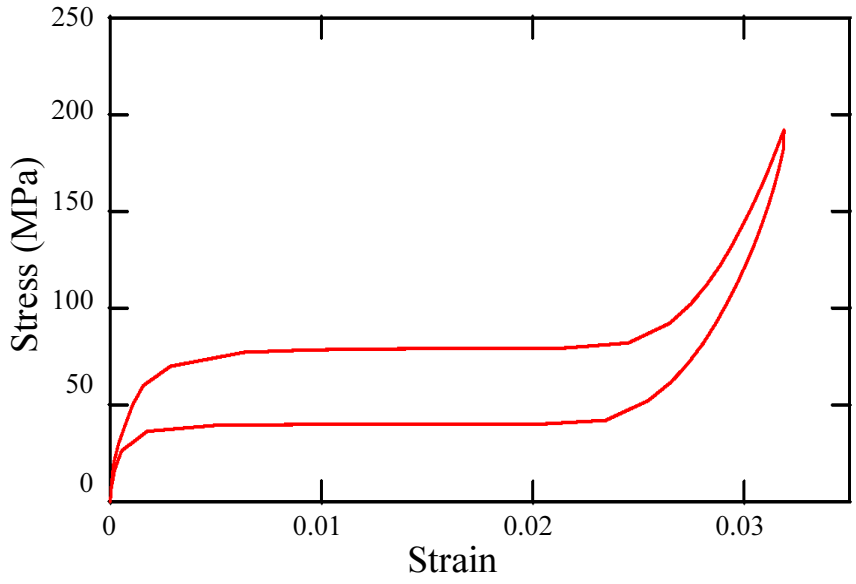

Figure 2: Numerical simulation obtained using the self-consistent approach for an isothermal tensile test on a polycrystalline pseudoelastic CuZnAl alloy. Computation performed at room temperature ($T = 20°C$), $A^f = 15°C$. Simulation results using the model of Gao and Brinson (2002).

remain partial in pseudoelasticity (existence of residual austenite). Similar saturation values are obtained by Gao and Brinson (2002) and have been observed experimentally in NiTi and CuAlMnZn polycrystalline specimens (Brinson et al., 2002a,b).

Numerical results confirm that the macroscopic mean transformation strain cannot be considered a constant parameter (Figure 4). This overall value rapidly decreases in the beginning of the loading and reaches a saturation value that depends on the loading state. The maximum value of $\bar{\varepsilon}^{tM}$ obtained in the very beginning of the transformation is equal to the transformation strain of the first-induced well-oriented variant.

Describing the strain mechanism at a microscopic length scale allows that the evolution of the microstructural parameters be obtained. In this approach, information such as the progress of the transformation inside each individual grain and the evolution of the different variants of martensite with respect to the loading path are obtained. This allows that two stages of the transformation be distinguished.

In the first stage, increase in the global martensitic volume fraction is mainly due to the increase in the number of grains in which the transformation takes place (Figure 5(a)). In stage two, all grains transform, but the number of variants per grain increases to reach an average saturation value close to three variants per grain as illustrated by Figure 5(b).

The model also takes into account the asymmetry observed in the behavior of these alloys for tensile and compression tests. The crystallographical origin of this phenomenon has been determined in the work of Patoor et al. (1995). The habit plane normal and the transformation direction serving as input data, it is natural that the asymmetry phenomenon is taken into account there. For the computed curves, the critical stress, the transformation slope and the hysteresis size are larger in compression than in tension (Figure 6 and Figure 7). This is in agreement with the experimental trends (Vacher and Lexcellent, 1991).

Considering different loading paths, a transformation surface in stress space can be determined (Figure 8). Symmetric behavior is obtained for shear loading which is in agreement with experimental observations (Manach, 1992). Analytical description of such a surface using the second and third invariants of the deviatoric stress tensor is useful in structural calculation (Gillet et al., 1995)).

2.3.3 Comparison with Experimental Observations

Numerical determination obtained using the proposed scale transition framework is now compared with experimental results on pseudoelastic CuZnAl alloys from the literature. The CuAl alloy used by Vacher and Lexcellent (1991) was provided by the Tréfimétaux company. The average grain size is 0.3 mm. The

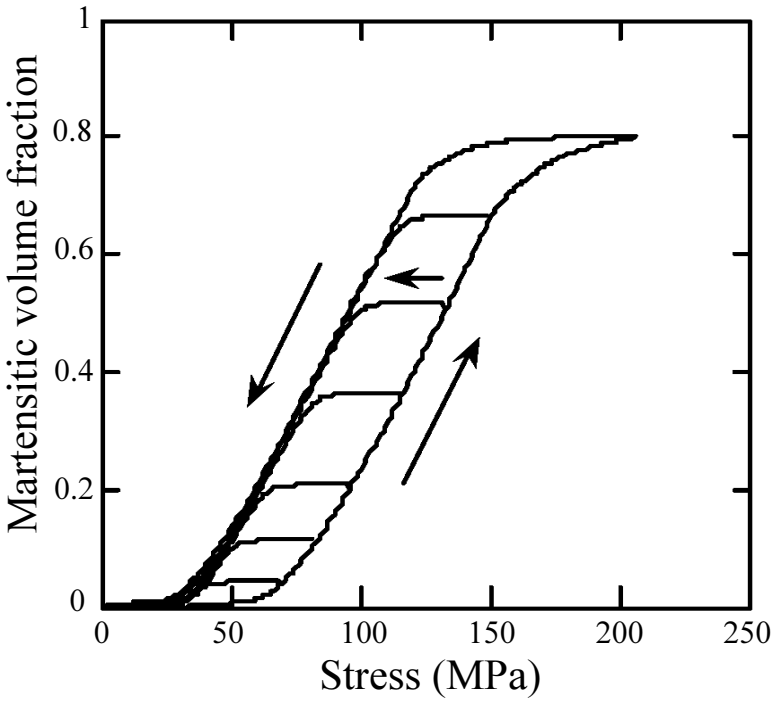

Figure 3: Kinetics of a stress-induced martensitic transformation numerically defined using the self-consistent simulation. The simulation is performed using the model by Patoor et al. (1996).

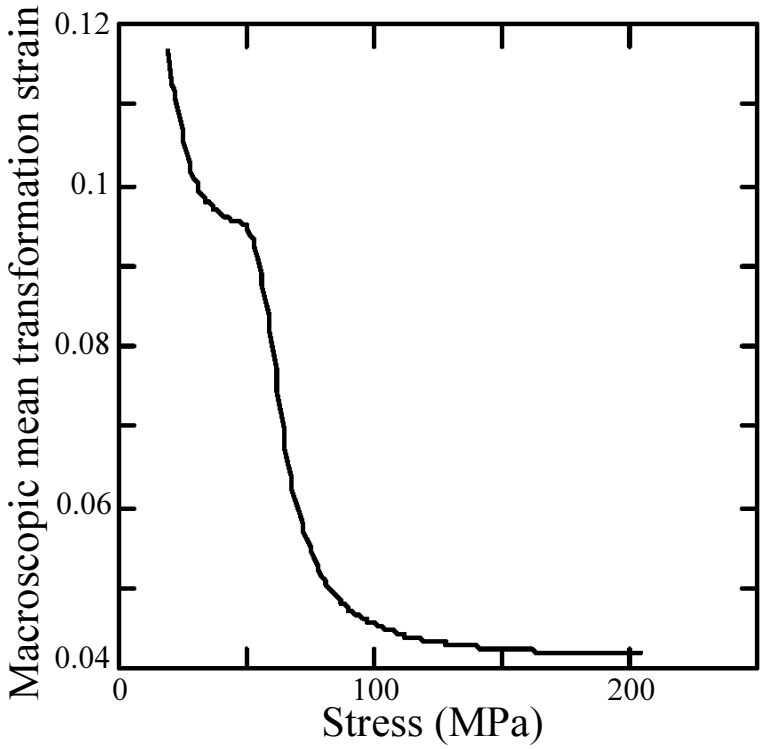

Figure 4: Evolution of the macroscopic mean transformation strain during a pseudoelastic tensile test (Entemeyer et al., 1995).

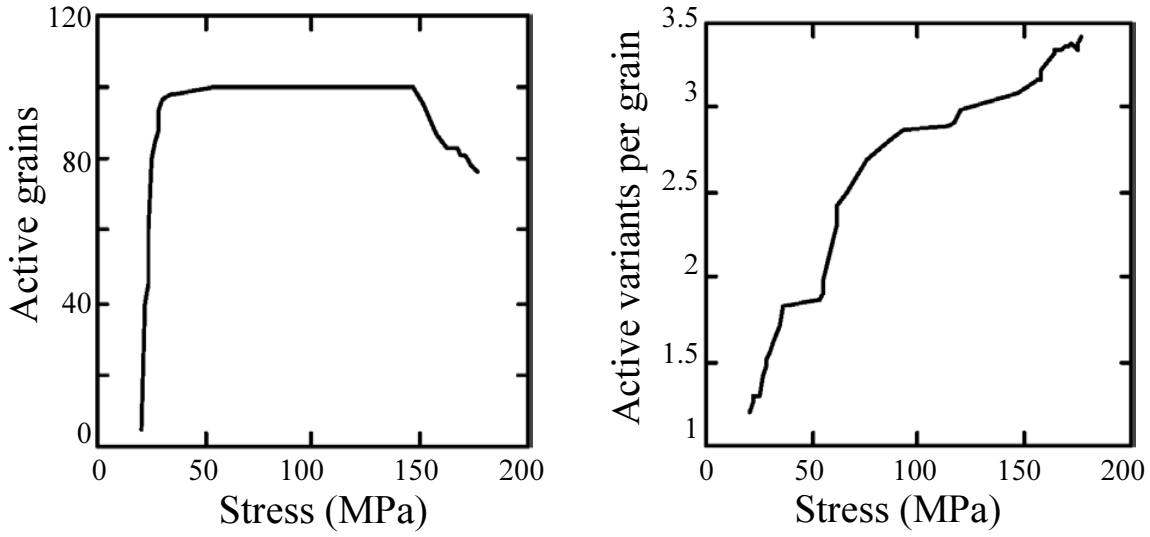

(a) (b)

Figure 5: (a) Evolution of the number of active grains during a tensile test; (b) Evolution of the number of active variants per grain on loading (Entemeyer et al., 1995).

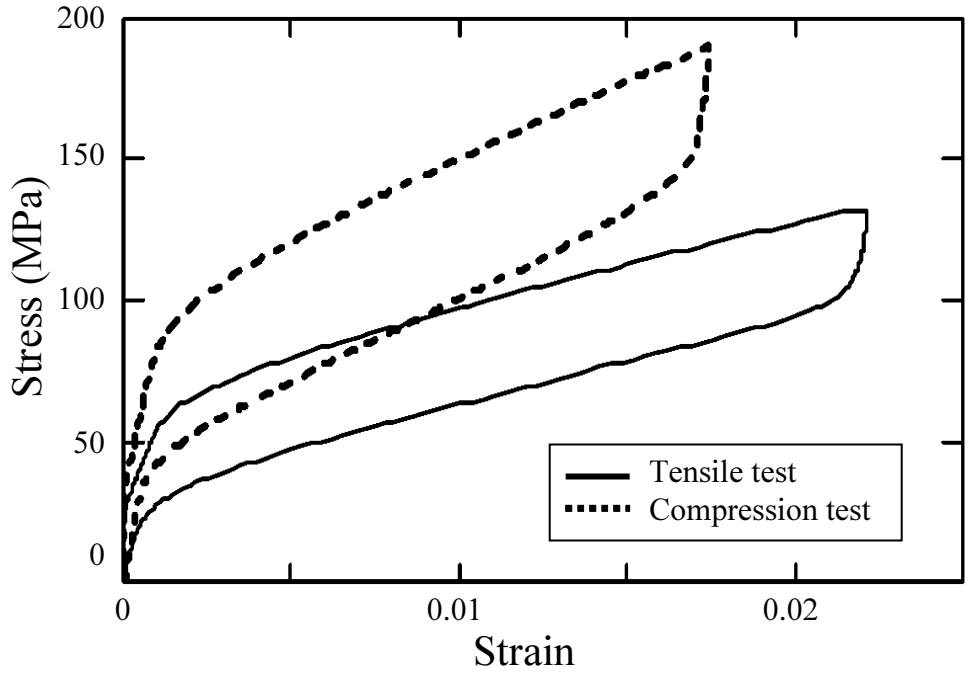

Figure 6: Asymmetry observed between tensile and compression tests as obtained by numerical simulation using the self-consistent approach ($T - M^s = 10°\text{C}$). Simulation using the model by Patoor et al. (1996).

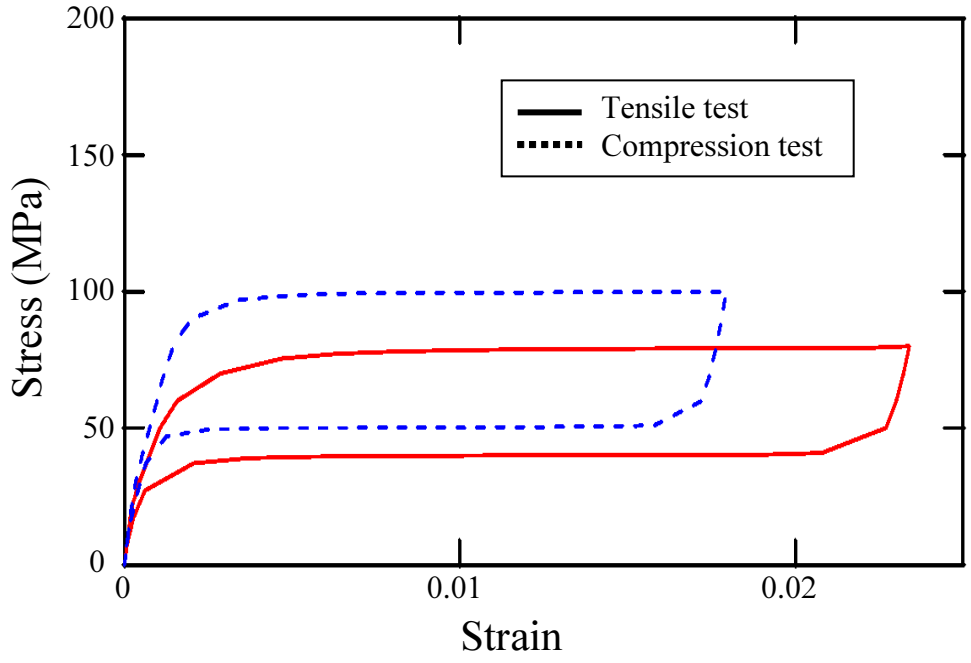

Figure 7: Asymmetry observed between tensile and compression tests as obtained by numerical simulation using the self-consistent approach ($T - M^s = 10°\text{C}$) (Gao and Brinson, 2002).

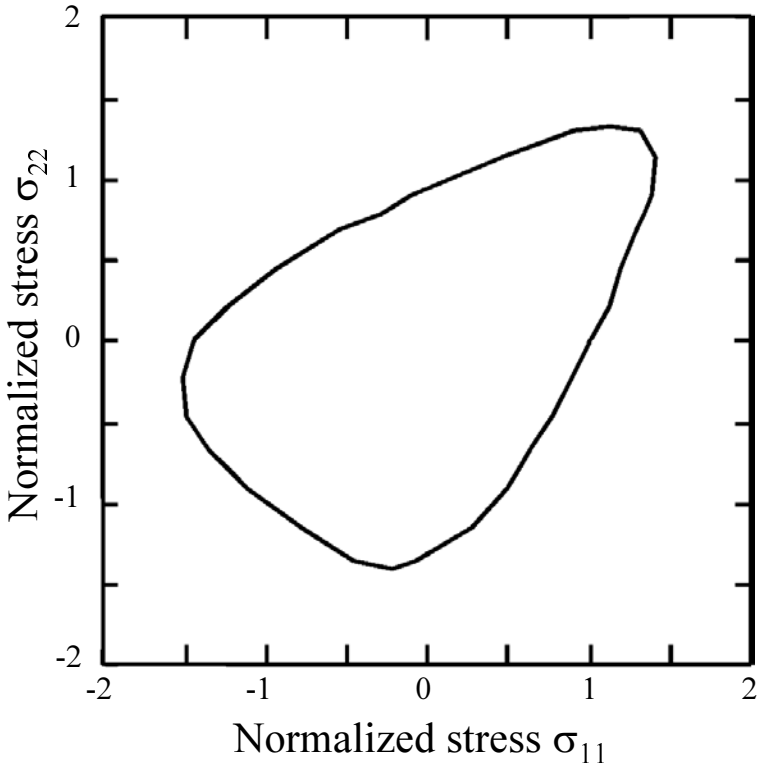

Figure 8: Asymmetrical 2-D transformation surface for SMAs in stress space numerically determined using the self-consistent approach (Patoor et al., 1995).

thermal treatment was as follows: solution heated in β-phase (10 minutes at 850°C), water-quenched and annealed at 20°C for 48 hours. The characteristic transformation temperatures are $M^s = -98$°C and $A^f = -91$°C (determined by a resistivity measurement). A uniaxial tensile test was performed on a specimen with a 10 mm $\times$ 0.6 mm rectangular cross-section and a length of 45 mm. Deformations were measured using an extensometer. The imposed strain rate was 10^{-4}s^{-1}. Variations in temperature were obtained using a thermally controlled chamber in which liquid nitrogen is vaporized. Vacher and Lexcellent (1991) characterized the pseudoelastic behavior of this alloy between -80°C and 100°C.

Numerical results obtained from the self-consistent model are determined using the same material parameters as those of the preceding section (n_i, m_i, γ, B, μ, H^{nm}). Particularities of the studied alloy are taken into account by the parameters T_0 and F_c. These quantities are determined from experimental measurements of the temperatures T, M^s and A^f given by Vacher and Lexcellent (1991). Comparison with an experimental tensile stress-strain curve for -80°C indicates that the transformation slope and the hysteresis size are correctly evaluated by the model (Figure 9). Two predictions by Gao and Brinson (2002) are included, one using identical B and F_c values as in Patoor et al. (1996) ($B = 0.23$, $F_c = 0.805$), and another using alternate B and F_c values ($B = 0.17$, $F_c = 0.644$) based on recent examination of single crystal data (Gao et al., 2000). One also notes hardening features especially between strain values of 0.003 and 0.006 which are due to the interaction of grains and their variants.

The computed and measured transformation stresses are in good agreement. In the same way, an increase of the test temperature maintains a good correspondence between computed and measured transformation stress (Figure 10) for a large range of test temperatures.

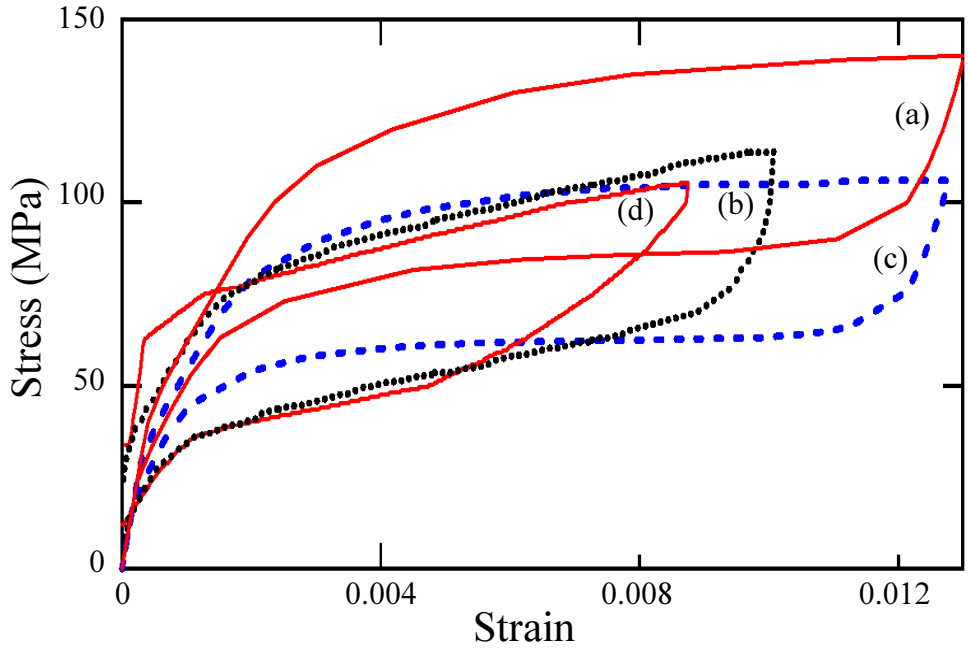

Figure 9: Comparisons of experimental observations (a) performed on a pseudoelastic CuZnAl alloy (Vacher and Lexcellent, 1991) with numerical simulations for three different models: (b) – Patoor et al. (1996); (c) – Gao and Brinson (2002); (d) – Gao and Brinson (2002) using the values for the parameters B and Fc (cf. part I) from Patoor et al. (1996).

Since the three-dimensional aspects of the martensitic transformation at the microscopic level are taken into account by the self-consistent method, the proposed framework can be applied to describe multiaxial loading paths. There are, however, only few experimental studies of the multiaxial behavior of shape memory alloys. Tensile-torsion tests were performed by Rogueda (1993) on a CuZnAl alloy provided by the Tréfimétaux company. This alloy was solution-treated in β-phase (15 minutes at 850°C), quenched and annealed at 120°C for one hour, and then kept at room temperature for several days. The characteristic transformation temperatures, determined by resistivity measurements, are $M^s = 14$°C and $A^f = 20$°C. Pseudoelastic tensile-torsion tests were performed on a tube with a diameter of 20 mm, a thickness of 2 mm and a length of 71 mm at a temperature of 30°C. Deformations were measured using LVDT and RVDT

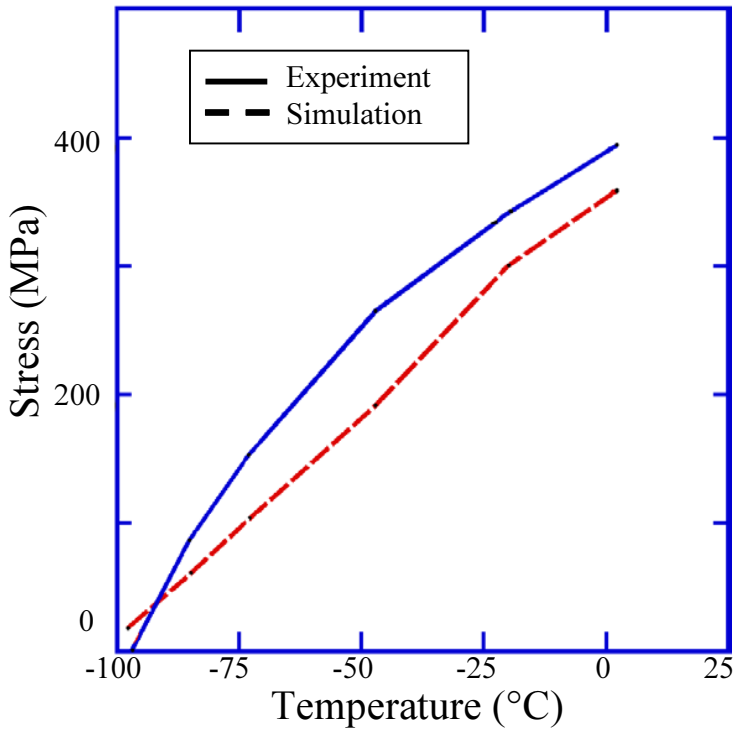

Figure 10: Critical stress for onset of stress-induced martensitic phase transformation in a CuZnAl alloy plotted as a function of temperature (Vacher and Lexcellent, 1991).

extensometer.

Different proportional loadings are performed, ranging from uniaxial tensile test to pure torsion, keeping the maximum Von Mises equivalent stress equal to 110 MPa. These experimental conditions were simulated using the self-consistent model. A very good agreement was obtained (Figure 11). The $r\theta$ and zz components of the stress-strain curve are well-captured by the simulation without any fitting parameter. Only the test conditions (applied stress and test temperature) and the characteristic temperatures (M^s and A^f) are changed in the input data. Change in the critical transformation stress due to the asymmetrical aspects in the pseudoelastic behavior is also well captured (Zirifi, 1994).

Non-isothermal behavior can also be described without adding a new internal parameter. The influence of a continuous change in the imposed temperature can be accounted for by deriving a complete thermo-mechanical integral equation for the scale transition problem as shown by Entemeyer et al. (1995). In this case, stress and temperature act like loading parameters. The anisothermal creep behavior of shape memory alloys is very well described using this extension of the model (see Figure 12) though the model of Gao and Brinson (2002) shows a more rapid transformation response.

Experimental results reported by Bourbon et al. (1995) on thermal cycling of a CuZnAl shape memory alloy under a constant applied stress of 65 MPa are well captured by this scale transition approach. Numerical results demonstrate that the decrease of the maximal transformation strain with the applied stress level, which has been experimentally observed, is related to the formation of self-accommodated structure inside the martensite phase.

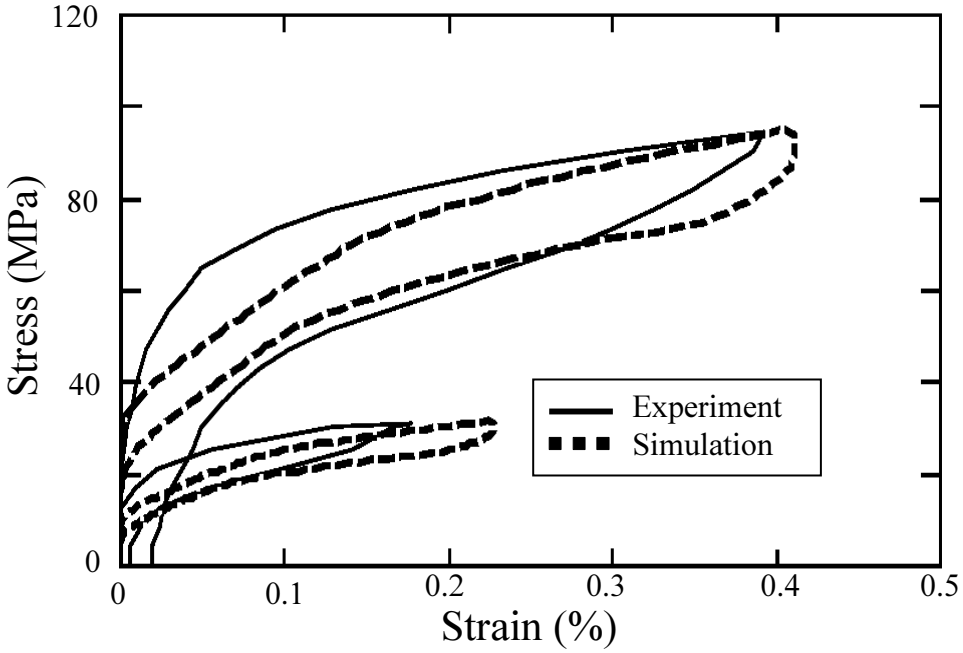

Figure 11: Pseudoelastic tensile-torsion test with $\sigma_{r\theta}/\sigma_{zz}$ ratio of 0.333 for a CuZnAl alloy. Comparison between experimental measurement performed by Rogueda (1993) and simulation obtained using the self-consistent method (Patoor et al., 1996).

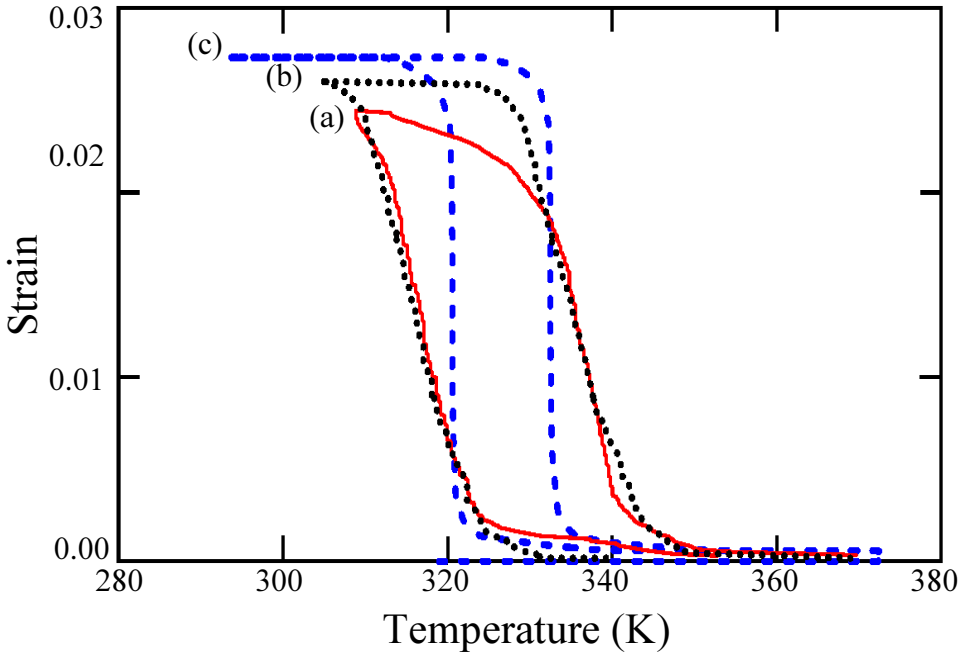

Figure 12: Thermally induced phase transformation in a CuZnAl alloy under constant stress of 65MPa, $M_s = 40$°C and $A_f = 52$°C; The experimental results (a) by Bourbon et al. (1995) are compared with two numerical simulations: (b) – Entemeyer et al. (1995); (c) – Gao and Brinson (2002).

3 Phenomenological Modeling of SMAs

In the case of the phenomenological models, a macroscopic free energy function that depends on internal variables and their evolution equations are usually postulated and used in conjunction with the second law of thermodynamics to derive constraints on the constitutive behavior of the SMA material. Thus the resulting models are not directly derived from specific microstructure. These models have the advantage of being easily integrated into a structural analysis computational framework, e.g., using the finite element method.

Describing the complex characteristics involved in the phase transitions in polycrystalline SMAs has been a significant challenge to researchers. These include modeling the hardening during phase transformation; the asymmetric response that SMAs exhibit in tension and compression; the modeling of detwinning of martensite and, more generally, complicated thermomechanical paths beyond isobaric or isothermal ones; two-way shape memory effect; the effects of reorientation and the accumulation of plastic strains during cyclic loading. Historically, the first subject addressed by researchers was the choice of transformation hardening functions. These topics have been covered in the review paper by Birman (1997). A detailed account can also be found in Lagoudas et al. (1996). In this paper the topic is briefly summarized in Section 3.1.1.

The topic of transformation surfaces (Section 3.1.2) and tension-compression asymmetry of the SMA response has been investigated by Raniecki and Lexcellent (1998) who presented a model for pseudoelasticity of SMAs. A distinct feature of the model is its capability to take into account the difference between the tension and compression loading. This is accomplished by using a $J_2 - J_3$ transformation surface. The model uses exponential hardening functions. It was used in a later work by Raniecki et al. (2001) to study bending of SMA beams undergoing pseudoelastic loading. In this particular work the tension-compression difference was neglected. The authors were able to determine the distribution of the martensitic volume fraction along the thickness of the beam during both loading and unloading. Additional results included plots of the beam curvature versus the applied moment. Rejzner et al. (2002) have further extended the work on pseudoelastic beams, by including the effect of tension-compression asymmetry in the analysis and comparing the results with experimental data. It was found, however, that the tension-compression asymmetry does not have a significant influence on the macroscopic beam response.

The comprehensive study of Qidwai and Lagoudas (2000b) focused on the choice of different transformation functions and their effect on the material response. In particular, the asymmetry of the material behavior under tension and compression, as well as the volumetric transformation strain, can be modeled by choosing an appropriate functional form of transformation function. Qidwai and Lagoudas (2000b) proposed a transformation function, based on the J_2, J_3 and I_1 stress invariants which can account for the observed asymmetry. The subject of the form of the transformation function has been revisited in a recent paper by Lexcellent et al. (2002). Multiaxial experiments on CuZnAl and CuAlBe polycrystalline SMAs have been performed to determine the initial transformation surface. The experiments have revealed tension-compression asymmetry, consistent with the results found in the literature. Motivated by the experimental results, Lexcellent et al. (2002) have proposed an analytical expression for the transformation function, based on the J_2 and J_3 stress invariants.

Another important aspect of the SMA response is the detwinning of martensite (Section 3.2). A 1-D model that separates the martensitic volume fraction into two parts: thermally-induced (self-accommodated) and stress-induced (detwinned) has been presented by Brinson (1993). Leclercq and Lexcellent (1996) have presented a similar model formulated in a 3-D framework; however, only 1-D implementation and numerical results have been provided. Comparisons are made with experimental data for both pseudoelastic mechanical loading as well for isobaric thermally-induced transformation. It has been found that the results are in reasonably good agreement, with the largest discrepancies observed for the case of isobaric thermally-induced transformation. In another study, Lagoudas and Shu (1999) have proposed a 3-D model with three internal variables but again with only 1-D numerical implementation and results. The main difference with the earlier model by Leclercq and Lexcellent (1996) is in the type of transformation hardening function.

One of the important problems recently addressed by the researchers is the behavior of SMAs under cycling loading (Tanaka et al. (1995); Lexcellent and Bourbon (1996); Fischer et al. (1998); Lexcellent et al. (2000); Abeyaratne and Kim (1997); Bo and Lagoudas (1999a,b,c); Lagoudas and Entchev (2004)). During cyclic phase transformation a substantial amount of plastic strains is accumulated. In addition, the transformation loop evolves with the number of cycles and TWSME is developed. Based on the experimental observations researchers have attempted to create models able to capture the effects of cycling loading. One-dimensional models for the behavior of SMA wires under cycling loading have been presented by Tanaka et al. (1995); Lexcellent and Bourbon (1996); Lexcellent et al. (2000) and Abeyaratne and Kim (1997), among others.

A series of papers by Bo and Lagoudas (1999a,b,c) and Lagoudas and Bo (1999) studies the cyclic behavior of SMA wires in one dimension. The work focuses on the modeling of stress-induced transformation, where both transformation and plastic strains occur simultaneously as a results of the applied stress. The resulting model is able to account for simultaneous development of transformation and plastic strains during phase transformation under applied loads. In addition to the plastic strain, the changes in the material response are also modeled by introducing evolution equations for the material parameters. Finally, minor hysteresis loops are also modeled by Bo and Lagoudas (1999c). This is accomplished by modifying the transformation criterion and the hardening parameters during a minor loop. All of the above-mentioned features of the model have been demonstrated and the results have been compared with experimental data for NiTi SMA wires. The results have been found to be in very good agreement.

A three-dimensional model for transformation induced plasticity has been presented by Fischer et al. (1998). In contrast to the work by Bo and Lagoudas (1999b), separate phase transformation condition and plasticity yield condition are used by Fischer et al. (1998). The theory is presented in general terms, but the identification of the material parameters and the implementation are not discussed.

Many other approaches to modeling SMAs have also been proposed. The work of Brocca et al. (2002) presents a three-dimensional model for SMAs which is based on the microplane model by Bažant (1984). The main idea of the model is to deduce the macroscopic constitutive behavior of an SMA by describing the response of the SMA along planes of different orientations, called *microplanes*. The SMA constitutive behavior on the microplanes is described by a one-dimensional model. First, the normal and shear components of the stress on each microplane are defined in terms of the unit normal and tangential vectors of the plane and the macroscopic stress tensor. Next, the normal and shear components of the strain are calculated based on the constitutive model for the microplane. Finally, the components of the macroscopic strain tensor are calculated from the normal and shear strain components for a set of microplanes using the principal of virtual work. The particular SMA constitutive model on the microplane implemented in the work by Brocca et al. (2002) is the one presented by Bekker and Brinson (1998), however, it is noted that any other model can easily be implemented. The effect of the hydrostatic pressure and the tension/compression asymmetry are also taken into account by modifying the critical stress values for phase transformation and the transformation temperatures. Various results demonstrating the capabilities of the microplane model are presented and compared with experimental data.

One of the latest one-dimensional models for SMA wires is presented by Shaw (2002). The model is capable of simulating both the pseudoelastic behavior and the shape memory effect. The new development of the model by Shaw (2002) is the accounting for the instabilities during martensitic phase transformation by including strain gradient effects and by allowing softening stress-strain response.

Different implementation issues for SMA constitutive models have been presented and discussed in a series of papers by Govindjee and coworkers (Govindjee and Kasper, 1999; Govindjee and Miehe, 2001; Hall and Govindjee, 2002). The model presented by Govindjee and Kasper (1999) is based on stress-temperature phase diagram for SMAs. The approach taken in that work is similar to the one presented by Bekker and Brinson (1997). It is assumed that during the martensitic phase transformation two different martensitic variants may form, depending on the sign of the applied loading. In addition, if the material is cooled in stress-free condition, both variants form simultaneously, resulting in zero macroscopic transformation strain. Further mechanical loading will result in growth of one martensitic variant at the expense of the other, thus producing observable macroscopic transformation strain in the direction of the loading. In a later work Govindjee and Hall (2000) present a constitutive model based on statistical physics. Similar to their previous work (Govindjee and Kasper, 1999) the evolution of two martensitic variants is prescribed. The model is numerically implemented and results for different loading conditions, including stress-induced and thermally-induced transformation are presented. A three-dimensional model for SMAs has been presented by Govindjee and Miehe (2001) and Hall and Govindjee (2002), where the number of martensitic variants formed during transformation is not restricted to two. The general equations of the model have been presented as well as its numerical implementation. The numerical results have been compared to experimental data for CuAlNi SMA (Shield, 1995). A summary of the features of some more commonly used SMA models is given in Table 3.

A general outline of how a typical phenomenological model is developed is given in the next Section 3.1, followed by the most common choices for transformation hardening function (Section 3.1.1) and transformation surfaces (Section 3.1.2). The problems involved in modeling of detwinning and reorientation are discussed in Section 3.2 and one particular modeling approach (Lagoudas and Entchev, 2004) to transformation induced plasticity is given in Section 3.3.

Table 3: Summary of phenomenological constitutive models. Unless otherwise specified, ξ is used to denote the volume fraction of all martensite, ξ^d the volume fraction of detwinned and ξ^t the volume fraction of twinned (self accommodated) martensite.

Model	**Formulation**	**Internal variables**	**Features**
			One dimensional models
Tanaka (1986)		ξ	Uses an exponential hardening rule for the phase transformation. Material properties remain constant during phase transformation.
Liang and Rogers (1990)	Helmholtz free energy	ξ	Uses a cosine hardening rule for the phase transformation. Material properties remain constant during phase transformation.
Brinson (1993)	Helmholtz free energy	ξ^t, ξ^d	Introduces two internal variables allowing modeling of both stress induced and self accommodated martensite. Uses a cosine hardening law and nonconstant elastic stiffness during phase transformation
Bekker and Brinson (1997, 1998)	Phase diagram based	ξ^t, ξ^d	The model is entirely formulated in terms of possible thermomechanical paths in stress-temperature space. Cosine hardening rule is used for the phase transformation.
Govindjee and Kasper (1999)	Phase diagram based	ξ^{M^+}, ξ^{M^-}	A distinction is made for martensitic variants in tension M^- and compression M^+. Constant stiffness and thermal expansion coefficient are assumed. The model also includes linear kinematic hardening plasticity. The plastic strains influence the total amount of martensite that can be produced through an exponential relation.
			Three dimensional models
Liang and Rogers (1992)	Helmholtz free energy	ξ	Three dimensional extension of Liang and Rogers (1990) based on a J_2 transformation surface
Boyd and Lagoudas (1994a)	Gibbs free energy, quadratic in ξ.	ξ	Uses the volume fraction of stress induced martensite as internal variable and a flow rule to connect it with the transformation strain. A J_2-type of transformation surface is used for the forward phase transformation. The model accounts for non-proportional loading paths by using a non-associative flow rule during reverse transformation.
Boyd and Lagoudas (1996a)	Gibbs free energy, quadratic in ξ.	ξ	Provides a unified framework and generalizes the earlier models of Tanaka (1986); Liang and Rogers (1990); Boyd and Lagoudas (1994a)
Leclercq and Lexcellent (1996)	Helmholtz free energy	ξ^t, ξ^d	Uses two internal variables to allow modeling of both stress induced and self accommodated martensite. All transformation surfaces are of J_2 type, as a result effects of reorientation during non-proportional loading cannot be captured. Exponential hardening is used for both the stress induced transformation and reorientation of martensite.
Raniecki and Lexcellent (1998)	Gibbs free energy	ξ	Models tension compression asymmetry using a $J_2 - J_3$ type transformation surface. Exponential transformation hardening functions are used.
Lexcellent et al. (2000)	Helmholtz free energy	ξ^t, ξ^d	An extension of the Leclercq and Lexcellent (1996) model which also accounts for the TWSME. This is done by modifying the free energy by an experimental expression depending on the maximum stress σ_{max} during training. This allows to capture the final result of the training but does not model the cycling loading process itself.
Bo and Lagoudas (1999a,b,c); Lagoudas and Bo (1999)	Gibbs free energy	ξ	Extends the work of Boyd and Lagoudas (1994a) to include modeling of transformation induced plasticity. This is done by introducing the following state variables: transformation strain, plastic strain, drag stress, back stress and connecting their evolution to the evolution of the martensitic volume fraction ξ. Only one-dimensional implementation of the transformation induced plasticity is given.

Model	Formulation	Internal variables	Features
Lagoudas and Shu (1999)	Gibbs free energy	$\xi^{A\leftrightarrow M^t}$, $\xi^{A\leftrightarrow M^d}$, $\xi^{M^t\rightarrow M^d}$	The model extends the earlier work of Boyd and Lagoudas (1994a). The polycrystalline SMA is considered a mixture of three species - self accommodated martensite M^t, detwinned martensite M^d and austenite A. The internal variables describe the three possible transitions between the different species. Nonproportional loading for pseudoelasticity is handled in the same way as in Boyd and Lagoudas (1994a). The model however cannot account for the simultaneous reverse transformation $M^t, M^d \rightarrow A$ and only a one-dimensional implementation is provided.
Qidwai and Lagoudas (2000b)	Gibbs free energy. Quadratic in ξ.	ξ	Comprehensive modeling of tension-compression asymmetry. An extension of the works by Boyd and Lagoudas (1994a, 1996a). Several different transformation surfaces based on I_1-, J_2- and J_3-type invariants are proposed.
Brocca et al. (2002)	Microplane based	N/A	The constitutive model on each microplane is the model by Brinson (1993). Thermal expansion is neglected and the elastic modulii are assumed constant for the two phases. The model is able to account for nonproportional loading paths.
Govindjee and Miehe (2001); Hall and Govindjee (2002)	Helmohltz/Gibbs free energy containing 3-rd and 4-th order polynomial terms of the internal variables	$\{\xi^i\}_{i=1}^n$, n is the number of variants	The paper generalizes earlier phenomenological models by considering an arbitrary number of martensitic variants n. The focus of the paper is the numerical implementation of the model via a nonlinear optimization method.
Juhasz et al. (2002)	Helmholtz, quadratic in the internal variables	$\boldsymbol{\varepsilon}^t$, ξ^t	The paper presents a novel approach at dealing with nonproportional loading. The effects of reorientation are taken into account by taking the entire transformation strain $\boldsymbol{\varepsilon}^t$ as an internal variable instead of the detwinned martensitic volume only. The thermodynamic forces remain nonzero after the completion of the phase transformation ($\xi = 1$) leading to change in the components of the transformation strain but not its magnitude.
Lagoudas and Entchev (2004)	Gibbs free energy	ξ	The model accounts for the simultaneous development of transformation and plastic strains during stress-induced phase transformation. The work extends and implements in 3-D the model presented in (Bo and Lagoudas, 1999a,b,c; Lagoudas and Bo, 1999).

3.1 General formulation

The general framework presented here follows the developments of Lagoudas et al. (1996); Qidwai and Lagoudas (2000b). The main idea is to formulate the (Gibbs) free energy of the SMA polycrystalline material as a weighted sum of the free energies of the austenitic and the martensitic phases plus the free energy of mixing:

$$G(\boldsymbol{\sigma}, T, \xi, \boldsymbol{\varepsilon}^t) = G^A(\boldsymbol{\sigma}, T) + \xi \left(G^M(\boldsymbol{\sigma}, T) - G^A(\boldsymbol{\sigma}, T) \right) + G^{\text{mix}}(\boldsymbol{\sigma}, T, \xi, \boldsymbol{\varepsilon}^t), \tag{3.1}$$

where $\boldsymbol{\sigma}$ is the Cauchy stress tensor, T is the temperature, ξ is the martensitic volume fraction, $\boldsymbol{\varepsilon}^t$ is the transformation strain tensor, G^A and G^M are the Gibbs free energies of the austenite and the martensite, respectively, and G^{mix} is the free energy of mixing. The following form for the Gibbs free energy for both phases is assumed:

$$G^A(\boldsymbol{\sigma}, T) = -\frac{1}{2\rho}\boldsymbol{\sigma} : \boldsymbol{\mathcal{S}}^A : \boldsymbol{\sigma} - \frac{1}{\rho}\bar{\boldsymbol{\alpha}}^A : \boldsymbol{\sigma}(T - T_0) + c^A \left[(T - T_0) - T \ln\left(\frac{T}{T_0}\right) \right] + s_0^A T + u_0^A, \tag{3.2}$$

$$G^M(\boldsymbol{\sigma}, T) = -\frac{1}{2\rho}\boldsymbol{\sigma} : \boldsymbol{\mathcal{S}}^M : \boldsymbol{\sigma} - \frac{1}{\rho}\bar{\boldsymbol{\alpha}}^M : \boldsymbol{\sigma}(T - T_0) + c^M \left[(T - T_0) - T \ln\left(\frac{T}{T_0}\right) \right] + s_0^M T + u_0^M, \tag{3.3}$$

where $\boldsymbol{\mathcal{S}}^i$, $\bar{\boldsymbol{\alpha}}^i$, c^i, s_0^i and u_0^i are the compliance tensor, thermal expansion coefficient tensor, specific heat, specific entropy and the specific internal energy at the reference state of the individual phases with the supperscript $i = A$ for austenitic and $i = M$ for martensite, respectively. Finally, ρ is the material density which is the same for both phases.

Further, a wide range of models can be presented within this formulation if the following assumption is made on the mixing term:

$$G^{\text{mix}} = -\frac{1}{\rho}\boldsymbol{\sigma} : \boldsymbol{\varepsilon}^t + \frac{1}{\rho} f(\xi), \tag{3.4}$$

where $f(\xi)$ is a generic function and ρ is the mass density. The fact that f is function of the martensitic volume fraction ξ only results in the hardening depending only on the amount of phase transformation. Combining equations (3.1)-(3.4), the free energy reduces to the following equation:

$$\begin{aligned} G(\boldsymbol{\sigma}, T, \xi, \boldsymbol{\varepsilon}^t) = &- \frac{1}{2\rho}\boldsymbol{\sigma} : \boldsymbol{\mathcal{S}}(\xi) : \boldsymbol{\sigma} - \frac{1}{\rho}\boldsymbol{\sigma} : \left[\bar{\boldsymbol{\alpha}}(\xi)(T - T_0) + \boldsymbol{\varepsilon}^t \right] \\ &+ c(\xi) \left[(T - T_0) - T \ln\left(\frac{T}{T_0}\right) \right] - s_0(\xi) T + u_0(\xi) + f(\xi), \end{aligned} \tag{3.5}$$

where $\boldsymbol{\mathcal{S}}(\xi)$, $\bar{\boldsymbol{\alpha}}(\xi)$, $c(\xi)$, $s_0(\xi)$ and $u_0(\xi)$ are the effective compliance tensor, thermal expansion coefficient tensor, specific heat, specific entropy and the specific internal energy at the reference state, respectively. The above effective material properties are calculated in terms of the martensitic volume fraction ξ using the rule of mixtures as

$$\mathbf{S}(\xi) = \mathbf{S}^A + \xi(\mathbf{S}^M - \mathbf{S}^A) = \mathbf{S}^A + \xi \Delta \mathbf{S}, \tag{3.6a}$$

$$\bar{\boldsymbol{\alpha}}(\xi) = \bar{\boldsymbol{\alpha}}^A + \xi(\bar{\boldsymbol{\alpha}}^M - \bar{\boldsymbol{\alpha}}^A) = \bar{\boldsymbol{\alpha}}^A + \xi \Delta \bar{\boldsymbol{\alpha}}, \tag{3.6b}$$

$$c(\xi) = c^A + \xi(c^M - c^A) = c^A + \xi \Delta c, \tag{3.6c}$$

$$s_0(\xi) = s_0^A + \xi(s_0^M - s_0^A) = s_0^A + \xi \Delta s_0, \tag{3.6d}$$

$$u_0(\xi) = u_0^A + \xi(u_0^M - u_0^A) = u_0^A + \xi \Delta u_0. \tag{3.6e}$$

Next, standard thermodynamics arguments (cf. e.g. Malvern (1969)) are employed to obtain the constitutive equations for the strain $\boldsymbol{\varepsilon}$ and the specific entropy s, as well as the local internal dissipation rate:

$$\boldsymbol{\varepsilon} = -\rho \frac{\partial G}{\partial \boldsymbol{\sigma}}, \tag{3.7}$$

$$s = -\frac{\partial G}{\partial T}, \tag{3.8}$$

$$\boldsymbol{\sigma} : \dot{\boldsymbol{\varepsilon}}^t - \rho \frac{\partial G}{\partial \xi}\dot{\xi} \geq 0. \tag{3.9}$$

For convenience, the generalized thermodynamic driving force obtained by taking a derivative of the energy G with respect to ξ is denoted by p (Qidwai and Lagoudas, 2000b):

$$p = -\rho\frac{\partial G}{\partial \xi} = \frac{1}{2}\boldsymbol{\sigma} : \Delta\mathbf{S}\boldsymbol{\sigma} + \boldsymbol{\sigma} : \Delta\bar{\boldsymbol{\alpha}}(T - T_0) - \rho\Delta c\left[T - T_0 - T\ln\left(\frac{T}{T_0}\right)\right] + \rho\Delta s_0(T - M_s). \tag{3.10}$$

At this stage of the constitutive modeling a transformation surface which separates the thermoelastic response region from the transformation region is defined:

$$\Phi = \begin{cases} \hat{\Phi}(\boldsymbol{\sigma}) + p - Y, & \dot{\xi} > 0, \\ -\hat{\Phi}(\boldsymbol{\sigma}) - p - Y, & \dot{\xi} < 0, \end{cases} \tag{3.11}$$

where Y is a material parameter. For a detailed discussion on the existence of a thermoelastic domain, the reader is referred to Rajagopal and Srinivasa (1998a). A general flow rule is also assumed to have the type:

$$\dot{\boldsymbol{\varepsilon}}^t = \boldsymbol{\Lambda}\dot{\xi}. \tag{3.12}$$

Here $\boldsymbol{\Lambda}$ has the meaning of a transformation direction tensor. Under these two assumptions the transformation function and the rate of the martensitic volume fraction must satisfy the Kuhn–Tucker conditions (Qidwai and Lagoudas, 2000b):

$$\begin{array}{lll} \dot{\xi} \geq 0, & \Phi \leq 0, & \Phi\dot{\xi} = 0, \\ \dot{\xi} \leq 0, & \Phi \leq 0, & \Phi\dot{\xi} = 0. \end{array} \tag{3.13}$$

Note that the equation (3.9) and the flow rule (3.12) imply

$$\boldsymbol{\sigma} : \dot{\boldsymbol{\varepsilon}}^t - \rho\frac{\partial G}{\partial \xi}\dot{\xi} = (\boldsymbol{\sigma} : \boldsymbol{\Lambda} - p)\,\dot{\xi} \geq 0, \tag{3.14}$$

that is, the thermodynamic force π conjugate to ξ is given by (Lagoudas et al., 1996; Qidwai and Lagoudas, 2000b):

$$\pi = \boldsymbol{\sigma} : \boldsymbol{\Lambda} - p. \tag{3.15}$$

To complete the constitutive model, the free energy of mixing $G^{\text{mix}}(\boldsymbol{\sigma}, T, \xi, \boldsymbol{\varepsilon}^t)$ in equation (3.1), the transformation surfaces by selecting the functional form for $\hat{\Phi}(\boldsymbol{\sigma})$, and the transformation flow rule $\boldsymbol{\Lambda}$ need to be defined. The mixing energy influences the transformation hardening during pseudoelastic loading and the motivation behind different choices proposed in the literature are discussed in the next Section 3.1.1. Different choices for $\hat{\Phi}(\boldsymbol{\sigma})$ and $\boldsymbol{\Lambda}$ are discussed in Section 3.1.2.

It is important to point out that a Clausius-Clapeyron type relation similar to equation (I-2.1) can be derived by considering the stress-temperature dependence of the transformation surfaces for a given volume fraction of martensite. Since in this formulation, the elastic compliances, thermal modulii and specific heat of austenite and martensite are allowed to differ, the resulting temperature dependence of the critical stress for initiation of phase transformation will depart from the linear relationship given by (I-2.1) (Bo and Lagoudas, 1999b; Qidwai and Lagoudas, 2000a).

3.1.1 Transformation hardening functions

It is a common assumption in the early constitutive models (Tanaka, 1986; Tanaka et al., 1986, 1995; Liang and Rogers, 1990, 1992; Brinson, 1993; Boyd and Lagoudas, 1994a, 1996a) that the hardening depends only on the amount of phase transformation, i.e., a specific form for $f(\xi)$ is selected in equation (3.4). The most general assumption is that it is different for the forward and reverse transformation:

$$f(\xi) = \begin{cases} f^M(\xi), & \dot{\xi} > 0, \\ f^A(\xi), & \dot{\xi} < 0. \end{cases} \tag{3.16}$$

The particular choice of $f(\xi)$ is governed by experimental observations. Depending on the chemical composition, heat treatment, mechanical training, etc, different choices have been made in the literature. For example, the exponential model of Tanaka (1986) chooses the functions f^M and f^A as follows

$$f^M = \frac{\rho\Delta s_0}{a_e^M}\left[(1-\xi)\ln(1-\xi) + \xi\right] + (\mu_1^e + \mu_2^e)\xi, \tag{3.17}$$

$$f^A = \frac{\rho\Delta s_0}{a_e^A}\xi\left[\ln(\xi) - 1\right] + (\mu_1^e - \mu_2^e)\xi, \tag{3.18}$$

where a_e^M, a_e^A, μ_1^e and μ_2^e are material parameters.

Liang and Rogers (1990), on the other hand have proposed

$$f^M = \int_0^\xi -\frac{\rho\Delta s_0}{a_c^M}\left[\pi - \cos^{-1}(2\hat{\xi}-1)\right]\mathrm{d}\hat{\xi} + (\mu_1^c + \mu_2^c)\xi, \tag{3.19}$$

$$f^A = \int_0^\xi -\frac{\rho\Delta s_0}{a_c^A}\left[\pi - \cos^{-1}(2\hat{\xi}-1)\right]\mathrm{d}\hat{\xi} + (\mu_1^c - \mu_2^c)\xi, \tag{3.20}$$

which, in a uniaxial tension test leads to a simple cosine hardening law. Here a_c^M, a_c^A, μ_1^c and μ_2^c are material parameters. In the polynomial model of Boyd and Lagoudas (1996a) a different form is proposed:

$$f^M = \frac{1}{2}\rho b^M \xi^2 + (\mu_1^p + \mu_2^p)\xi, \tag{3.21}$$

$$f^A = \frac{1}{2}\rho b^A \xi^2 + (\mu_1^p - \mu_2^p)\xi, \tag{3.22}$$

where b^M, b^A, μ_1^p and μ_2^p are material constants.

3.1.2 Transformation Surfaces

The motivation for selecting different transformation functions is the observed tension-compression asymmetry of SMA materials as well as the development of a small volumetric strain during phase transformations.

Before considering specific choices for the transformation function $\hat{\Phi}(\boldsymbol{\sigma})$ the implications of the principle of maximum transformation dissipation are considered (Rajagopal and Srinivasa, 1998b; Qidwai and Lagoudas, 2000b). It can be shown (Qidwai and Lagoudas, 2000b) that this principle implies an associative flow rule. That is, the transformation direction tensor in equation (3.12) is the derivative with respect to stress of the transformation function:

$$\boldsymbol{\Lambda} = \frac{\partial\hat{\Phi}(\boldsymbol{\sigma})}{\partial\boldsymbol{\sigma}}, \tag{3.23}$$

In such a case, the choice of $\boldsymbol{\Lambda}$ cannot be independent of $\Phi(\boldsymbol{\sigma})$. Notice the transformation flow rule (3.12) with the special form of $\boldsymbol{\Lambda}$ given in equation (3.23) is associative in temperature-stress space, but not in stress space only.

In practice, by selecting only a single internal volume fraction the effects of martensitic reorientation cannot be accounted for by an associative flow rule for both loading and unloading. It can happen that after following a non-proportional pseudoelastic loading path, upon unloading there will be residual strain. To avoid this situation, it is often assumed that the transformation flow rule during unloading is not associative (with regard to the transformation surface, i.e. in stress-temperature space). An example is the model of Lagoudas et al. (1996), where the transformation function is selected as

$$\hat{\Phi}(\boldsymbol{\sigma}) = \sqrt{\frac{3}{2}}H||\mathrm{dev}(\boldsymbol{\sigma})||. \tag{3.24}$$

Here, $\mathrm{dev}(\boldsymbol{\sigma}) = \boldsymbol{\sigma} - \frac{1}{3}\mathrm{tr}(\boldsymbol{\sigma})\mathbf{I}$ is the deviatoric stress and $||\cdot||$ is the tensor scalar product. They further assume maximum transformation dissipation during loading, which implies

$$\boldsymbol{\Lambda} = \sqrt{\frac{3}{2}}H\frac{\mathrm{dev}(\boldsymbol{\sigma})}{||\mathrm{dev}(\boldsymbol{\sigma})||}, \quad \text{for } \dot{\xi} > 0, \tag{3.25}$$

In the above equations, H is the maximum uniaxial transformation strain. Note also, that $\sqrt{\frac{3}{2}}||\mathrm{dev}(\boldsymbol{\sigma})||$ is the von Mises stress. The transformation direction tensor during unloading however is assumed of the form

$$\boldsymbol{\Lambda} = \frac{\boldsymbol{\varepsilon}_{\mathrm{rev}}^t}{\xi_{\mathrm{rev}}}, \quad \text{for } \dot{\xi} < 0. \tag{3.26}$$

The quantities $\boldsymbol{\varepsilon}_{\mathrm{rev}}^t$ and ξ_{rev} are the transformation strain and the martensitic volume fraction at the beginning of the reverse phase transformation. Equation (3.26) implies that the transformation strain at the end of a pseudoelastic thermomechanical loading path is always zero.

For the remainder of this section the particular choices of forward transformation surface will be considered an associative transformation flow rules (3.23) will be assumed. This topic is studied at length by Qidwai and Lagoudas (2000b). In particular, it is shown, that the asymmetry of the material behavior under tension and compression as well as the volumetric transformation strain can be modeled by choosing an appropriate transformation function. The authors demonstrate that a variety of transformation surface with different characteristics can be obtained by choosing a particular functional form of $\hat{\Phi}(\boldsymbol{\sigma})$ in equation (3.11). If the function $\hat{\Phi}(\boldsymbol{\sigma})$ is J_2-based[1] (von Mises type) such as

$$\hat{\Phi}(\boldsymbol{\sigma}) = \alpha\sqrt{3J_2}, \tag{3.27}$$

then the transformation function used by Boyd and Lagoudas (1996a) is recovered. The transformation direction tensor $\boldsymbol{\Lambda}$ in this case will have the following form (cf. equation (3.25)):

$$\boldsymbol{\Lambda} = \frac{3}{2}\alpha\frac{\mathrm{dev}(\boldsymbol{\sigma})}{||\mathrm{dev}(\boldsymbol{\sigma})||}. \tag{3.28}$$

It can be seen from equations (3.25) and (3.28) that the parameter α is identified with the maximum transformation strain H.

Another choice of the function $\hat{\Phi}(\boldsymbol{\sigma})$ involves both J_2 and I_1 invariants:

$$\hat{\Phi}(\boldsymbol{\sigma}) = \beta\sqrt{3J_2} + \gamma I_1. \tag{3.29}$$

The resulting transformation direction tensor is given by

$$\boldsymbol{\Lambda} = \frac{3}{2}\beta\frac{\mathrm{dev}(\boldsymbol{\sigma})}{||\mathrm{dev}(\boldsymbol{\sigma})||} + \gamma\mathbf{1}, \tag{3.30}$$

where $\mathbf{1}$ is second order identity tensor. The parameter β is similar to the parameter α in equation (3.27), while the parameter γ is used to model either the volumetric transformation strain or the tension-compression asymmetry. As noted by Qidwai and Lagoudas (2000b), if γ is used to account for the tension-compression asymmetry, then the predicted volumetric transformation strain may be erroneous. Therefore, to avoid this problem, a third transformation function, based on the J_2, J_3 and I_1 stress invariants is proposed. The function $\hat{\Phi}(\boldsymbol{\sigma})$ takes the following form:

$$\hat{\Phi}(\boldsymbol{\sigma}) = \eta\sqrt{3J_2}\left[1 + \nu\frac{J_3}{(3J_2)^{3/2}}\right] + \omega I_1. \tag{3.31}$$

It is also noted that for certain choice of the parameters the transformation surface may become non-convex. The resulting transformation direction tensor has the form

$$\boldsymbol{\Lambda} = \eta\left[\frac{3\mathrm{dev}(\boldsymbol{\sigma})}{2\sqrt{3J_2}} + \nu\frac{\sqrt{3J_2}\,(\mathrm{dev}(\boldsymbol{\sigma})\mathrm{dev}(\boldsymbol{\sigma}) - {}^2\!/_3 J_2\mathbf{1}) - 3J_3\mathrm{dev}(\boldsymbol{\sigma})}{(3J_2)^2}\right] + \omega\mathbf{1}, \tag{3.32}$$

where $\mathbf{1}$ is a second-order identity tensor.

The material constant ω is equal to one-third of the volumetric transformation strain while the constants η and ν are calibrated using the maximum transformation strains in tension (H^t) and compression (H^c).

The SMA constitutive model presented by Souza et al. (1998) can be derived as a special case of the model by Qidwai and Lagoudas (2000b). Two different transformation functions were used by Souza et al. (1998). The first transformation function is based on the J_2 stress invariant and was used to simulate uniaxial loading. The second transformation function was introduced to accommodate torsional loading and is based on J_2 and I_1 invariants. However, as shown by Qidwai and Lagoudas (2000b) the use of the I_1 stress invariant may lead to large volumetric transformation strain, not observed in the experiments. This issue is not discussed in the work of Souza et al. (1998). The constitutive model by Souza et al. (1998) was numerically implemented using return mapping algorithms. The numerical results obtained for non-proportional loading have been presented and compared with experimental data by Šittner et al. (1995).

The subject of the form of the transformation function has been revisited in an recent paper by Lexcellent et al. (2002). Multiaxial experiments on CuZnAl and CuAlBe polycrystalline SMAs have been performed to

[1] J_2 is the second deviatoric stress invariant defined as $J_2 = \frac{1}{2}\mathrm{dev}(\boldsymbol{\sigma}) : \mathrm{dev}(\boldsymbol{\sigma})$, J_3 is the third deviatoric stress invariant defined as $J_3 = \det(\mathrm{dev}(\boldsymbol{\sigma}))$ and I_1 is the first stress invariant, $I_1 = \mathrm{tr}(\boldsymbol{\sigma})$.

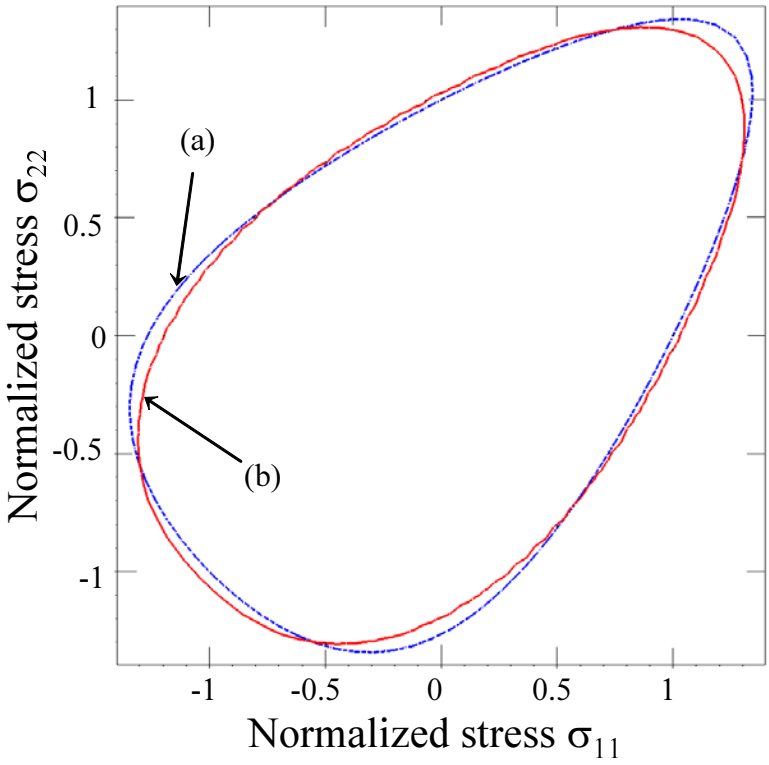

Figure 13: Initial transformation surfaces obtained by Lexcellent et al. (2002) – (a) and Qidwai and Lagoudas (2000b) – (b).

determine the initial transformation surface. The experiments have revealed tension-compression asymmetry, consistent with the results found in the literature. Motivated by the experimental results, Lexcellent et al. (2002) have proposed an analytical expression for the transformation function, based on the J_2 and J_3 stress invariants. The function has the form

$$\tilde{\Phi} = \alpha\sqrt{3J_2}F(y), \tag{3.33}$$

where

$$y = \frac{27}{2}\frac{J_3}{(3J_2)^{3/2}}, \tag{3.34}$$

$$F(y) = \cos\left(\frac{\arccos(1-a(1-y))}{3}\right) \tag{3.35}$$

and a is a parameter. The choice of the function $F(y)$ has been made to avoid non-convexity of the transformation surface. However, as seen from Figure 13 the transformation surfaces obtained using equation (3.31) and equation (3.35) have very similar shape. Furthermore, the transformation surfaces shown in Figure 13 closely resemble the transformation surface obtained using micromechanical modeling and shown in Figure 8. Note that the stresses in both Figures 8 and 13 are normalized by the critical uniaxial tensile stress σ^{Ms}, however the two figures are not drawn to the same scale.

3.2 Detwinning of martensite and effects of reorientation

Aiming at creating a model which accounts both for the stress-induced martensite and detwinning, Leclercq and Lexcellent (1996) have separated the martensitic volume fraction into two part: thermally-induced (self-accommodated) and stress-induced (detwinned). It should be mentioned, however, that similar approach has been presented earlier by Brinson (1993). Next, Leclercq and Lexcellent (1996) have introduced transformation criteria for both types of martensite, as well as criterion for detwinning. The transformation criterion for the stress-induced transformation is based on the J_2 stress invariant (von Mises type, see equation (3.29)).

An exponential transformation hardening function has been used by Leclercq and Lexcellent (1996). One-dimensional numerical results for three different types of alloys have been presented and compared them with experimental data for both pseudoelastic mechanical loading as well for isobaric thermally-induced transformation. It has been found that the results are in reasonably good agreement, with the largest discrepancies observed for the case of isobaric thermally-induced transformation.

A different approach to the same problem is presented by Bekker and Brinson (1997) and Bekker and Brinson (1998). A one-dimensional constitutive model for SMA wires/rods is formulated in terms of a phase diagram description of the possible thermomechanical loading paths in stress-temperature space. In the first of the two papers, Bekker and Brinson (1997) presented the detailed derivation of the model. Each loading path is divided into segments where forward/reverse phase transformation or neutral loading occurs. Thus the transformation onset, finish, and reversal points are defined. Then, for each segment of the loading path a kinetic equation is applied to update the martensitic volume fraction, depending on the direction of the loading. The kinetic equations used by Bekker and Brinson (1997) are similar to the cosine model first proposed by Liang and Rogers (1990), while it is also mentioned that any other kinetic equations can be used, e.g., an exponential (Tanaka, 1986) or polynomial (Boyd and Lagoudas, 1996a) kinetic law. The second paper of this series (Bekker and Brinson, 1998) adopts the same approach presented in the first part, with emphasis given on different implementations for minor hysteresis loops, which occur due to incomplete forward/reverse transformation. Three different algorithms for handling minor hysteresis loops are implemented and analyzed. Numerical examples for different loading paths have been presented and discussed. While attractive for one-dimensional applications, it is difficult to generalize this approach to three dimensions.

An attempt to create a three dimensional model that accounts both for stress induced martensite as well as for detwinning is performed in Lagoudas and Shu (1999). The polycrystalline SMA is considered a mixture of three species - self accommodated martensite M^t, detwinned martensite M^d and austenite A. The three possible transitions are associated with different flow rules (the self accommodated transition does not produce any transformation strain) thus it is necessary to keep track of the amount of material that underwent each possible transition. The internal variables therefore describe the three possible transitions between the different species: $\xi^{A\leftrightarrow M^t}$, $\xi^{A\leftrightarrow M^d}$, $\xi^{M^t\rightarrow M^d}$. Nonproportional loading for pseudoelasticity is handled in the same way as in Boyd and Lagoudas (1994a). The model however cannot account for the simultaneous reverse transformation $M^t, M^d \rightarrow A$ and only a one-dimensional implementation is provided.

A polycrystalline material which undergoes stress-induced martensitic transformation under multiaxial loading exhibits reorientation of the martensitic variants. Thus, even in the case when the parent phase has transformed into some of the 24 martensitic variants, a change in the load direction certain unfavorable variants will transform to others in order to accommodate the loading conditions. This, however, will not produce additional transformation strain or change the overall volume fraction of martensite. Phenomenological models which consider single martensitic volume fraction as an internal variable are severely constrained in modeling reorientation of martensite. They must necessarily use non-associative transformation flow rules to accomplish that (cf. eg. Qidwai and Lagoudas (2000b)). An ad-hoc way of taking reorientation into account is to use a non-associative flow rule during unloading, such as the one given by equation (3.26), so that there is no residual transformation strain at the end of reverse transformation. An alternative way of accounting for reorientation is to consider the volume fraction of all possible martensitic variants, which is not feasible as it must provide a huge number of phenomenologically determined flow rules for the possible martensitic transformations. In a recent paper by Juhasz et al. (2002) an alternative approach that accounts for pseudoelasticity, detwinning, and reorientation is presented. The model does not couple the evolution of the martensitic volume fraction and inelastic strains as in equation (3.12) but instead uses the transformation strain $\boldsymbol{\varepsilon}^t$ and the volume fraction of self-accommodated martensite ξ^d as independent internal variables. The evolution equations for the internal variables are selected so that upon unloading the transformation strain becomes zero. While the model avoids dealing with an excessive number of internal variables, it is still more complex than models based on the volume fractions of twinned and detwinned martensite and its robustness is difficult to asses without numerical implementation and testing on a variety of thermomechanical paths.

3.3 Transformation Induced Plasticity

Here the approach taken in one of the most recent works on the cyclic behavior of SMAs (Lagoudas and Entchev, 2004) is briefly outlined. The work is an extension to the work of Bo and Lagoudas (1999a,b,c); Lagoudas and Bo (1999) to 3-D. The formulation of all of these models is based on the framework provided by Lagoudas et al. (1996), by introducing additional internal state variables, such as back and drag stress

and plastic strain. Following the notation of Section 3.1, the Gibbs free energy for the polycrystalline SMA is again given by equation (3.1), but the mixing term is modified to accommodate the plastic strain $\boldsymbol{\varepsilon}^p$, drag stresses η and back stresses $\boldsymbol{\alpha}$:

$$G^{\text{mix}} = -\frac{1}{\rho}\boldsymbol{\sigma}\left(\boldsymbol{\varepsilon}^t + \boldsymbol{\varepsilon}^p\right) - \frac{1}{\rho}\int_0^{\xi}\left[\boldsymbol{\alpha}\frac{\partial\boldsymbol{\varepsilon}^p}{\partial\hat{\xi}} + \eta\right]\mathrm{d}\hat{\xi} + G_0^{\text{ch}} + G^{\text{p}}. \tag{3.36}$$

The quantities G_0^{ch} and G^{p} are the Gibbs chemical free energy and the interaction energy induced by plastic strains in the austenite, respectively.

In addition to using additional terms in the mixing energy, a dependence of the maximum transformation strain on the level of the applied stress is also introduced, which leads to the following expression for the transformation strain direction coefficient $\boldsymbol{\Lambda}$:

$$\boldsymbol{\Lambda} = \begin{cases} \sqrt{\frac{3}{2}}H^{\text{cur}}\frac{\text{dev}(\boldsymbol{\sigma}^{\text{eff}})}{||\text{dev}(\boldsymbol{\sigma}^{\text{eff}})||}, & \dot{\xi} > 0, \\ \frac{\boldsymbol{\varepsilon}^t_{\text{rev}}}{\xi_{\text{rev}}}, & \dot{\xi} < 0. \end{cases} \tag{3.37}$$

The effective stress $\boldsymbol{\sigma}^{\text{eff}}$ is defined in terms of the applied stress $\boldsymbol{\sigma}$ and the back stress $\boldsymbol{\alpha}$ as

$$\boldsymbol{\sigma}^{\text{eff}} = \boldsymbol{\sigma} + \boldsymbol{\alpha}. \tag{3.38}$$

H^{cur} is the maximum uniaxial transformation strain, which depends on the value of the effective stress σ^{eff}. The training of the polycrystalline SMA and the evolution of the two-way shape memory effect is taken into account by introducing evolution equations for the back stress. The higher values of the back stress results in higher values for the maximum transformation strain even at low values of the applied stress.

It is noted that the plastic strain in the work of Bo and Lagoudas (1999b); Lagoudas and Entchev (2004) differs from plastic strain in conventional metal plasticity as it occurs at stress levels mush lower than the plastic yield limit. It is a direct result of the martensitic transformation and the microstructural changes caused by the transformation cycling. To model it, a new internal variable ζ^d having the meaning of accumulated detwinned martensitic volume fraction is introduced. It is connected to the evolution of the detwinned martensitic volume fraction $\dot{\xi}^d$ by

$$\zeta^d = \int_0^t |\dot{\xi}^d(\tau)|\mathrm{d}\tau. \tag{3.39}$$

The evolution equation for the plastic strain is assumed to be of the form (Lagoudas and Entchev, 2004)

$$\dot{\boldsymbol{\varepsilon}}^p = \boldsymbol{\Lambda}^p\dot{\zeta}^d, \tag{3.40}$$

where $\boldsymbol{\Lambda}^p$ is the plastic direction tensor. The following functional form of $\boldsymbol{\Lambda}^p$, which takes into account the saturation of the plastic strain during cyclic loading is used:

$$\boldsymbol{\Lambda}^p = \begin{cases} \sqrt{\frac{3}{2}}C_1^p\frac{\text{dev}(\boldsymbol{\sigma}^{\text{eff}})}{||\text{dev}(\boldsymbol{\sigma}^{\text{eff}})||}\exp\left(-\frac{\zeta^d}{C_2^p}\right), & \dot{\xi} > 0, \\ \sqrt{\frac{3}{2}}C_1^p\frac{\boldsymbol{\varepsilon}^t_{\text{rev}}}{||\varepsilon^t_{\text{rev}}||}\exp\left(-\frac{\zeta^d}{C_2^p}\right), & \dot{\xi} < 0, \end{cases} \tag{3.41}$$

The material parameters C_1^p and C_2^p govern the saturation value as well as the number of cycles necessary for the plastic strain to saturate.

To illustrate the capabilities of this model to handle cyclic loading, a set of results are presented for both uniaxial and multiaxial loading cases. As an example of uniaxial, results for large diameter NiTi wires under cyclic mechanical loading are shown in Figures 14 and 15. The wires are subjected to 20 loading cycles with a constant maximum value of stress.

The capabilities of the model to handle loading cases beyond uniaxial loading are demonstrated by modeling the response of an SMA torque tube. The stress-strain response of the tube is shown in Figure 16 where the average shear stress in the finite element is plotted versus the average shear strain. The results shown here are in qualitative agreement with the results reported by Lim and McDowell (1999). Since a

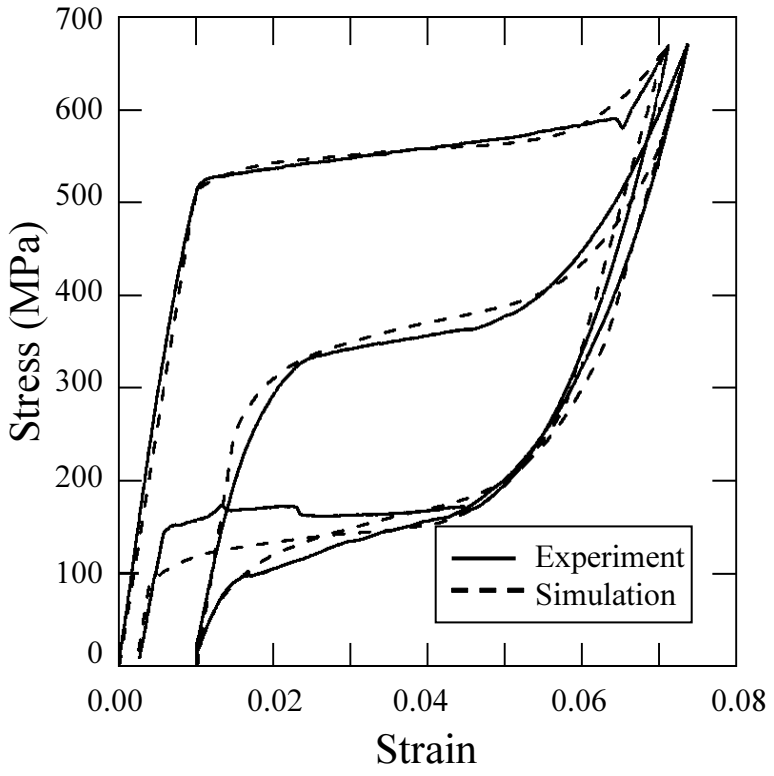

Figure 14: Stress-strain response demonstrating the effects of transformation induced plasticity. Given are comparison of the model simulations (Lagoudas and Entchev, 2004) with experimental data for the first and 20-th cycle.

full set of material parameters is not reported in the original work of Lim and McDowell (1999), the results cannot be compared quantitatively. It can be seen from the results that the hysteresis loop evolves with the number of loading cycles. One significant difference, observed between these results and the uniaxial results shown in Figures 14 and 15 is the value of the plastic strain at the end of the cycling test. While the final value of the plastic strain in the uniaxial test is equal to the value of the accumulated plastic strain, the final value in the case of torsional loading is significantly smaller. This result can be explain as follows: in the case of torsional cycling loading the direction of the loading is reversed during each cycle. Therefore, during each half of the loading cycle the direction of the plastic strain accumulation is also reversed. The result of this effect, as shown in Figure 17 is small total plastic strain. It should be noted, however, that even in the presence of small observable plastic strain the material still changes during the cycling. As seen from Figure 16 the hysteresis loop evolves during the cycling loading. Thus, the microstructural changes caused by the cyclic loading are taken into account by evolving the material parameters and updating the internal state variables.

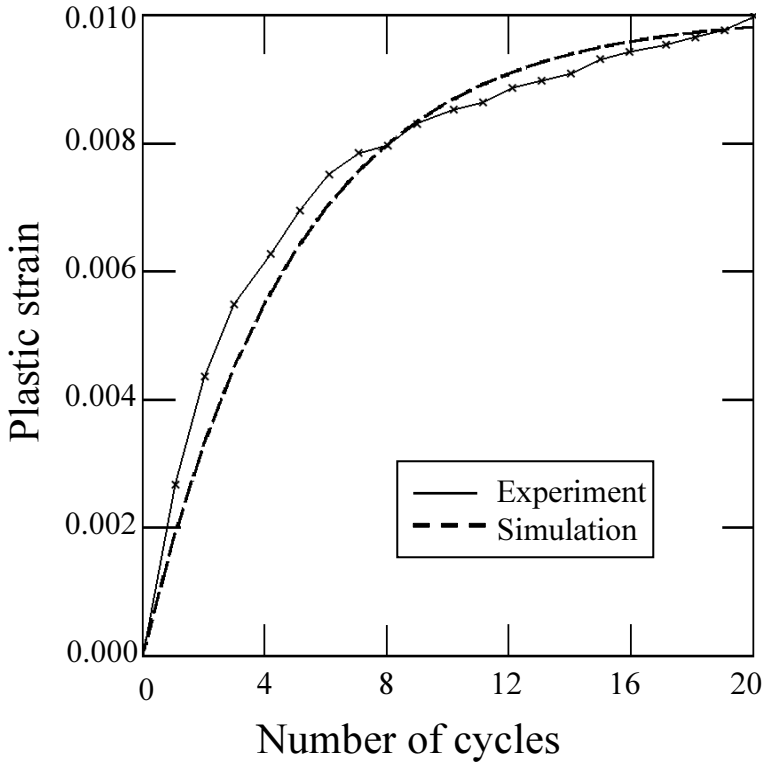

Figure 15: Evolution of plastic strain during constant maximum stress cycling (Lagoudas and Entchev, 2004).

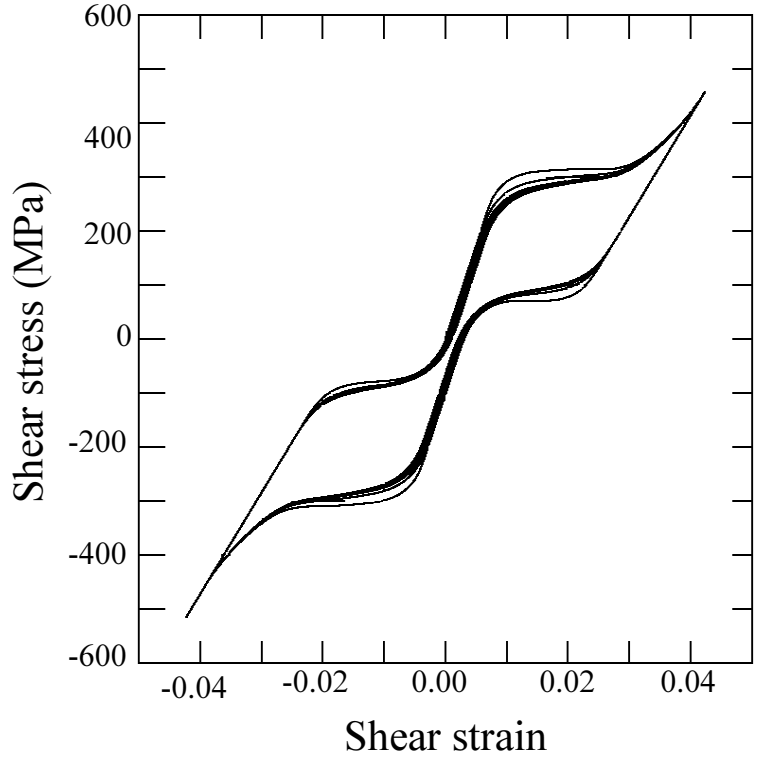

Figure 16: Stress-strain response of NiTi SMA tube subjected to cycling torsional loading: *average* shear stress over *average* shear strain (Lagoudas and Entchev, 2004).

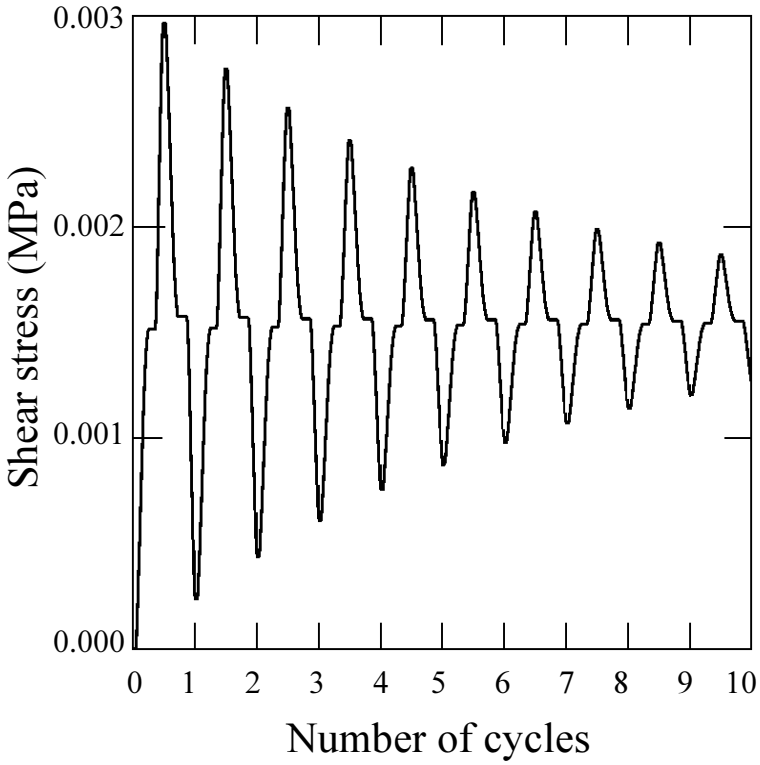

Figure 17: Plastic strain evolution in NiTi SMA tube during cycling torsional loading (Lagoudas and Entchev, 2004).

4 Numerical Implementation of SMA Constitutive Models

In this section the numerical implementation of thermomechanical constitutive equations is presented. The structure of the governing equations of an SMA constitutive model are very similar to the structure of the equations describing classical rate-independent plasticity. Therefore it is natural to utilize return-mapping algorithms developed for rate-independent plasticity (cf. e.g. Ortiz and Popov (1985); Ortiz and Simo (1986); Simo and Hughes (1998)) and apply them to SMAs.

Return mapping algorithms have been studied extensively over the years in the context of elasto-plasticity for the integration of constitutive relations. They are also called elastic predictor-plastic corrector algorithms where a purely (thermo) elastic trial loading is followed by a plastic corrector phase (return mapping). The corrector part is only applied if the stress state after the predictor step violates the plastic yield condition (transformation surface for the case of SMAs). The corrector enforces continuity iteratively in a manner consistent with the prescribed flow rule. Return mapping algorithms may differ on the basis of the kind of discretization employed to numerically integrate the evolution differential equations for the flow rule and the iterative procedure adopted to solve the resultant set of non-linear algebraic equations in the corrector part. Some commonly used return mapping algorithms proposed in the literature are the radial return (backward Euler based) algorithm (Wilkins, 1964) and the mean normal (mid-point rule based) algorithm (Rice and Tracey, 1973). A detailed review of the historical developments of the return mapping algorithms can be found in (Simo and Hughes, 1998).

Ortiz and Popov (1985) have observed that most of the return mapping algorithms employ integration rules that are particular cases of the trapezoidal and midpoint rules, suitably generalized to facilitate satisfaction of the plastic consistency condition. The stability of these integration algorithms for inelasticity is studied by Argyris et al. (1979); Simo and Govindjee (1991). The general conclusion is that backward integration strategies provide good stability of the incremental solution. Additional accuracy can be obtained by midpoint integration technique or by higher order approximation of the inelastic flow rule, for example by Runge-Kutta methods.

There are several differences between standard plastic materials and SMAs. SMAs have multiple transformation surfaces, e.g. forward and reverse stress-induced phase transformation as well as detwinning, if the model includes it. The surfaces are defined in both stress and temperature space. The reverse transformation surface is typically non-convex, which presents certain uniqueness issues discussed in Qidwai and Lagoudas (2000b). A typical flow rule such as the one for the forward transformation in equation (3.26) is not associative in stress space but becomes associative in stress-temperature space. In addition, the material properties - compliance, thermal expansion coefficient, specific entropy and internal energy involved in the constitutive relationship change during the transformation (cf. equations (3.6)) which results in additional complications in the numerical implementation. Also, unlike plasticity, the phase transformation ends after which the loading proceeds elastically. This imposes an additional constraint of the form $\xi \leq 1$ which needs to be addressed as well.

Extensive research on return mapping algorithms for SMAs has only recently been performed by Qidwai and Lagoudas (2000a) who have implemented return-mapping algorithms for the family of SMAs models (Tanaka, 1986; Tanaka et al., 1986, 1995; Liang and Rogers, 1990, 1992; Brinson, 1993; Boyd and Lagoudas, 1994a, 1996a). Two algorithms are developed - the closest point projection algorithm Ortiz and Pinsky (1981) and convex cutting plane algorithm (Simo and Ortiz, 1985; Ortiz and Simo, 1986). The difference between the two algorithms is in the corrector part. The application of the closest point projection algorithm results in a set of non-linear algebraic equations solved using Newtons iteration method. The closest point algorithm is unconditionally stable provided the yield surface is convex, and it is first-order accurate (Ortiz and Pinsky, 1981). On the other hand, the convex cutting plane method uses a Newton method only for the transformation surface and is based an explicit integration of the transformation flow rule. As a result it is computationally less demanding, however it is not unconditionally stable. While the work of Qidwai and Lagoudas (2000a) is focused on a single volume fraction of martensite, Govindjee and Miehe (2001) have focused on the numerical implementation by return mapping algorithms of models with multiple martensitic variants and, correspondingly, internal variables. In order to satisfy a polytope constraint an active set search strategy is proposed which determines the active variants and the corresponding thermoelastic prediction. The transformation correction is performed by the backward Euler method. The works considered above are all set up within the framework of infinitesimal strains. Auricchio et al. (1997); Auricchio (2001) have focused on adapting SMA constitutive models to finite strains and the have proposed a series of return-mapping algorithms based on the backward euler integration scheme for the transformation correction.

In this section, the major steps of the numerical implementation of the more recent model by Lagoudas and

Entchev (2004) are briefly outlined. The implementation can be viewed as an extension to the implementation of the earlier class of models described in Boyd and Lagoudas (1996a) for which the reader is referred to Qidwai and Lagoudas (2000a). The model uses a single volume fraction for the martensitic phase.

For the sake of improved readability, the model of Lagoudas and Entchev (2004) is summarized next. Equation (3.7) implies that the strain $\boldsymbol{\varepsilon}$ is given by

$$\boldsymbol{\varepsilon} = \boldsymbol{\mathcal{S}}(\xi) : \boldsymbol{\sigma} + \bar{\boldsymbol{\alpha}}(\xi)(T - T_0) + \boldsymbol{\varepsilon}^t + \boldsymbol{\varepsilon}^p. \tag{4.1}$$

The evolution equations (3.12) and (3.40) for the transformation strain $\boldsymbol{\varepsilon}^t$ and the plastic strain $\boldsymbol{\varepsilon}^p$ are given again for convenience

$$\dot{\boldsymbol{\varepsilon}}^t = \boldsymbol{\Lambda}\dot{\xi}, \tag{4.2}$$

$$\dot{\boldsymbol{\varepsilon}}^p = \boldsymbol{\Lambda}^p\dot{\zeta}^d, \tag{4.3}$$

where $\boldsymbol{\Lambda}$ and $\boldsymbol{\Lambda}^p$ are defined by equations (3.37) and (3.41) respectively. The transformation function Φ is defined as

$$\Phi = \begin{cases} \pi - Y, & \dot{\xi} > 0, \\ -\pi - Y, & \dot{\xi} < 0. \end{cases} \tag{4.4}$$

In the above equation π is the thermodynamic force conjugate to ξ and is given by

$$\begin{aligned} \pi = \frac{1}{2}\boldsymbol{\sigma} : \Delta\boldsymbol{\mathcal{S}} : \boldsymbol{\sigma} + \boldsymbol{\sigma} : \Delta\bar{\boldsymbol{\alpha}}(T - T_0) + \boldsymbol{\sigma} : \frac{\partial\boldsymbol{\varepsilon}^t}{\partial\xi} + \boldsymbol{\alpha} : \frac{\partial\boldsymbol{\varepsilon}^t}{\partial\xi} + \eta \\ - \rho\Delta c\left[T - T_0 - T\ln\left(\frac{T}{T_0}\right)\right] + \rho\Delta s_0(T - M^{0s}), \end{aligned} \tag{4.5}$$

Finally, ζ^d is connected to ξ by equation (3.39) and the evolution of the martensitic volume fraction ξ is constrained by the Kuhn–Tucker conditions:

$$\begin{aligned} &\dot{\xi} \geq 0, \quad \Phi \leq 0, \quad \Phi\dot{\xi} = 0, \\ &\dot{\xi} \leq 0, \quad \Phi \leq 0, \quad \Phi\dot{\xi} = 0. \end{aligned} \tag{4.6}$$

Thus the final system of nonlinear differential-algebraic equations consists of equations (4.1)–(4.3) along with the constraint (4.6).

4.1 Closest Point Projection Return Mapping Algorithm for SMA Constitutive Model

As mentioned above, the implementation of the SMA model is focused on a single material point. Further, the history of all field and internal variables at this material point is known. In particular, the values of $\boldsymbol{\varepsilon}_n$, T_n, $\boldsymbol{\sigma}_n$, $\boldsymbol{\varepsilon}^p_n$, ξ_n and ζ^d_n are known. The subscript n is used to denote a history/time parameter[2]. The new values of $\boldsymbol{\varepsilon}_{n+1}$ and T_{n+1} for the strain and temperature respectively are also given[3]. We must compute the values for $\boldsymbol{\sigma}_{n+1}$, $\boldsymbol{\varepsilon}^t_{n+1}$, $\boldsymbol{\varepsilon}^p_{n+1}$, ξ_{n+1} and ζ^d_{n+1} by solving equations (4.1)–(4.3) along with the constraint (4.6).

To solve this system, the evolution equations (4.2), (4.3) for the transformation and plastic strains are discretized as follows:

$$\boldsymbol{\varepsilon}^t_{n+1} = \boldsymbol{\varepsilon}^t_n + (\xi_{n+1} - \xi_n)\boldsymbol{\Lambda}_{n+1}, \tag{4.7}$$

$$\boldsymbol{\varepsilon}^p_{n+1} = \boldsymbol{\varepsilon}^p_n + (\zeta^d_{n+1} - \zeta^d_n)\boldsymbol{\Lambda}^p_{n+1}. \tag{4.8}$$

This type of forward Euler discretization is referred to as *the closest point projection* return mapping algorithm (Qidwai and Lagoudas, 2000a). The stress-strain relation (4.1) can also be written as

$$\boldsymbol{\sigma}_{n+1} = \boldsymbol{\mathcal{S}}(\xi_{n+1})^{-1} : \left(\boldsymbol{\varepsilon}_{n+1} - \boldsymbol{\varepsilon}^t_{n+1} - \boldsymbol{\varepsilon}^p_{n+1} - \bar{\boldsymbol{\alpha}}(\xi_{n+1})(T_{n+1} - T_0)\right). \tag{4.9}$$

In order to solve the discrete system (4.7)–(4.9) subject to the constraint (4.6) it is convenient to introduce the residual functions:

$$\mathbf{R}^t(\boldsymbol{\varepsilon}^t_{n+1}, \boldsymbol{\Lambda}_{n+1}, \xi_{n+1}) = -\boldsymbol{\varepsilon}^t_{n+1} + \boldsymbol{\varepsilon}^t_n + \boldsymbol{\Lambda}_{n+1}(\xi_{n+1} - \xi_n), \tag{4.10}$$

[2]For a quasi-static problem, this would be the values at the n-th loading step, while in a dynamic problem this would be the values of the field and internal variables at some discrete instance of time t_n.

[3]Alternatively, the increments $\Delta\boldsymbol{\varepsilon}_{n+1} = \boldsymbol{\varepsilon}_{n+1} - \boldsymbol{\varepsilon}_n$ and $\Delta T_{n+1} = T_{n+1} - T_n$ are given, which is equivalent to knowing $\boldsymbol{\varepsilon}_{n+1}$ and T_{n+1}.

$$\mathbf{R}^p(\boldsymbol{\varepsilon}^p_{n+1}, \boldsymbol{\Lambda}^p_{n+1}, \zeta^d_{n+1}) = -\boldsymbol{\varepsilon}^p_{n+1} + \boldsymbol{\varepsilon}^p_n + \boldsymbol{\Lambda}^p_{n+1}\left(\zeta^d_{n+1} - \zeta^d_n\right). \tag{4.11}$$

Observe, that (4.7) and (4.8) are equivalent to

$$\mathbf{R}^t(\boldsymbol{\varepsilon}^t_{n+1}, \boldsymbol{\Lambda}_{n+1}, \xi_{n+1}) = 0, \quad \mathbf{R}^p(\boldsymbol{\varepsilon}^p_{n+1}, \boldsymbol{\Lambda}^p_{n+1}, \zeta^d_{n+1}) = 0 \tag{4.12}$$

respectively.

The nonlinear algebraic system of equations (4.12),(4.9) subject to the constraint (4.6) is solved by constructing a converging iterative sequence

$$\boldsymbol{\sigma}^{(k)}_{n+1} \underset{k\to\infty}{\longrightarrow} \boldsymbol{\sigma}_{n+1}, \quad \boldsymbol{\varepsilon}^{t(k)}_{n+1} \underset{k\to\infty}{\longrightarrow} \boldsymbol{\varepsilon}^t_{n+1}, \quad \boldsymbol{\varepsilon}^{p(k)}_{n+1} \underset{k\to\infty}{\longrightarrow} \boldsymbol{\varepsilon}^p_{n+1}, \quad \xi^{(k)}_{n+1} \underset{k\to\infty}{\longrightarrow} \xi_{n+1}, \quad \zeta^{d(k)}_{n+1} \underset{k\to\infty}{\longrightarrow} \zeta^d_{n+1}. \tag{4.13}$$

As the first step, a **thermoelastic prediction** is performed during which, the internal variables do not change:

$$\boldsymbol{\varepsilon}^{t(0)}_{n+1} = \boldsymbol{\varepsilon}^t_n, \tag{4.14a}$$

$$\boldsymbol{\varepsilon}^{p(0)}_{n+1} = \boldsymbol{\varepsilon}^p_n, \tag{4.14b}$$

$$\xi^{(0)}_{n+1} = \xi_n, \tag{4.14c}$$

$$\zeta^{d(0)}_{n+1} = \zeta^d_n, \tag{4.14d}$$

$$\boldsymbol{\sigma}^{(0)}_{n+1} = \boldsymbol{\mathcal{S}}(\xi_n) - 1 : \left[\boldsymbol{\varepsilon}_{n+1} - \boldsymbol{\varepsilon}^{t(0)}_{n+1} - \boldsymbol{\varepsilon}^{p(0)}_{n+1} - \bar{\boldsymbol{\alpha}}(\xi_n)(T_{n+1} - T_0)\right], \tag{4.14e}$$

It should be noted, that this first step corresponds to purely thermoelastic loading without any transformation ($\dot{\xi} = 0$), hence its name thermoelastic prediction. The corresponding value of the transformation function Φ is then evaluated:

$$\Phi^{(0)}_{n+1} = \Phi(\boldsymbol{\sigma}^{(0)}_{n+1}, T_{n+1}, \xi^{(0)}_{n+1}). \tag{4.15}$$

If the value of the transformation function satisfies the transformation criterion $\Phi^{(0)}_{n+1} \leq 0$ then all equations and constraints are satisfied and the iteration is terminated for $k = 0$.

However, if the transformation criterion is violated, i.e., $\Phi^{(0)}_{n+1} > 0$ then a **transformation correction** is performed during which the stress and the internal variables are modified in accordance with the transformation flow rules and transformation consistency condition. That is, one has to solve (4.12) along with equation (4.9). The constraint (4.6) also needs to be satisfied, which, for $\dot{\xi} = \xi_{n+1} - \xi_n \neq 0$ is equivalent to

$$\Phi(\boldsymbol{\sigma}_{n+1}, T_{n+1}, \xi_{n+1}) = 0. \tag{4.16}$$

This is done by Newton's method: *For the given k-th iterate of* $\boldsymbol{\sigma}^{(k)}_{n+1}$, $\boldsymbol{\varepsilon}^{t(k)}_{n+l}$, $\boldsymbol{\Lambda}^{(k)}_{n+l}$, $\xi^{(k)}_{n+l}$, $\boldsymbol{\varepsilon}^{p(k)}_{n+l}$, $\boldsymbol{\Lambda}^{p(k)}_{n+l}$ *and* $\zeta^{d(k)}_{n+l}$ *find the* $k+1$ *iterates by linearizing* $\mathbf{R}^t$ *around* $\left(\boldsymbol{\varepsilon}^{t(k)}_{n+l}, \boldsymbol{\Lambda}^{(k)}_{n+l}, \xi^{(k)}_{n+l}\right)$, $\mathbf{R}^p$ *around* $\left(\boldsymbol{\varepsilon}^{p(k)}_{n+l}, \boldsymbol{\Lambda}^{p(k)}_{n+l}, \zeta^{d(k)}_{n+l}\right)$ *and* Φ *around* $\left(\boldsymbol{\sigma}^{(k)}_{n+1}, \xi^{(k)}_{n+1}\right)$ *and requiring that*

$$\mathbf{R}^{t(k)}_{n+1} - \left(\boldsymbol{\varepsilon}^{t(k+1)}_{n+1} - \boldsymbol{\varepsilon}^{t(k)}_{n+1}\right) + \left(\xi^{(k)}_{n+1} - \xi_n\right)\left(\boldsymbol{\Lambda}^{(k+1)}_{n+1} - \boldsymbol{\Lambda}^{(k)}_{n+1}\right) + \boldsymbol{\Lambda}^{(k)}_{n+1}\left(\xi^{(k+1)}_{n+1} - \xi^{(k)}_{n+1}\right) = 0, \tag{4.17}$$

$$\mathbf{R}^{p(k)}_{n+1} - \left(\boldsymbol{\varepsilon}^{p(k+1)}_{n+1} - \boldsymbol{\varepsilon}^{p(k)}_{n+1}\right) + \left(\zeta^{d(k)}_{n+1} - \zeta^d_n\right)\left(\boldsymbol{\Lambda}^{p(k+1)}_{n+l} - \boldsymbol{\Lambda}^{p(k)}_{n+1}\right) + \boldsymbol{\Lambda}^{p(k+1)}_{n+1}\left(\zeta^{d(k+1)}_{n+1} - \zeta^{d(k)}_{n+1}\right) = 0, \tag{4.18}$$

$$\Phi^{(k)}_{n+1} + \partial_{\boldsymbol{\sigma}}\Phi^{(k)}_{n+1} : \left(\boldsymbol{\sigma}^{t(k+1)}_{n+1} - \boldsymbol{\sigma}^{t(k)}_{n+1}\right) + \partial_\xi \Phi^{(k)}_{n+1}\left(\xi^{(k+1)}_{n+1} - \xi^{(k)}_{n+1}\right) = 0. \tag{4.19}$$

where $\mathbf{R}^{t(k)}_{n+1} = \mathbf{R}^t\left(\boldsymbol{\varepsilon}^{t(k)}_{n+1}, \boldsymbol{\Lambda}^{(k)}_{n+1}, \xi^{(k)}_{n+1}\right)$, $\mathbf{R}^{p(k)}_{n+1} = \mathbf{R}^p\left(\boldsymbol{\varepsilon}^{p(k)}_{n+1}, \boldsymbol{\Lambda}^{p(k)}_{n+1}, \zeta^{d(k)}_{n+1}\right)$ *and* $\Phi^{(k)}_{n+1} = \Phi\left(\boldsymbol{\sigma}^{(k)}_{n+1}, T_{n+1}, \xi^{(k)}_{n+1}\right)$.

The details of solving the linear system (4.17)-(4.19) are omitted, among which the elimination of ζ^d in the above equations in favor of ξ^d and ξ, the evaluation of the derivatives of the transformation tensors $\boldsymbol{\Lambda}$ and $\boldsymbol{\Lambda}^p$ or the computation of consistent tangent stiffness and thermal modulii. Instead, a summary of all steps of the numerical algorithm is given in Table 4. For details of all the derivations, the reader is referred to Entchev (2002).

Table 4: Summary of the closest point projection numerical algorithm for the SMA constitutive model (Entchev, 2002; Lagoudas and Entchev, 2004).

1. Let $k=0$, $\boldsymbol{\varepsilon}_{n+1}=\boldsymbol{\varepsilon}_n+\Delta\boldsymbol{\varepsilon}_{n+1}$, $T_{n+1}=T_n+\Delta T_{n+1}$, $\boldsymbol{\varepsilon}_{n+1}^{t(0)}=\boldsymbol{\varepsilon}_n^t$, $\boldsymbol{\varepsilon}_{n+1}^{p(0)}=\boldsymbol{\varepsilon}_n^p$, $\xi_{n+1}^{(0)}=\xi_n$, $\boldsymbol{\mathcal{S}}_{n+1}^{(0)}=\boldsymbol{\mathcal{S}}_n$, $\bar{\boldsymbol{\alpha}}_{n+1}^{(0)}=\bar{\boldsymbol{\alpha}}_n$.
2. Calculate $\boldsymbol{\sigma}_{n+1}^{(k)}$, $\Phi_{n+1}^{(k)}$, $\mathbf{R}_{n+1}^{t(k)}$, $\mathbf{R}_{n+1}^{p(k)}$:
$$\begin{aligned}
\boldsymbol{\sigma}_{n+1}^{(k)} &= \boldsymbol{\mathcal{S}}_{n+1}^{(k)-1}:\left[\boldsymbol{\varepsilon}_{n+1}-\boldsymbol{\varepsilon}_{n+1}^{t(k)}-\boldsymbol{\varepsilon}_{n+1}^{p(k)}-\bar{\boldsymbol{\alpha}}_{n+1}^{(k)}(T_{n+1}-T_0)\right]\\
\Phi_{n+1}^{(k)} &= \Phi(\boldsymbol{\sigma}_{n+1}^{(k)},T_{n+1},\xi_{n+1}^{(k)})\\
\mathbf{R}_{n+1}^{t(k)} &= -\boldsymbol{\varepsilon}_{n+1}^{t(k)}+\boldsymbol{\varepsilon}_n^t+\boldsymbol{\Lambda}_{n+1}^{(k)}(\xi_{n+1}^{(k)}-\xi_n)\\
\mathbf{R}_{n+1}^{p(k)} &= -\boldsymbol{\varepsilon}_{n+1}^{p(k)}+\boldsymbol{\varepsilon}_n^p+\boldsymbol{\Lambda}_{n+1}^{p(k)}\left|\xi_{n+1}^{d(k)}-\xi_n^d\right|
\end{aligned}$$
If $\Phi_{n+1}^{(k)}<0$ OR $\left|\Delta\xi_{n+1}^{(k)}\right|<TOL1$ then go to 7.
3. Calculate $\boldsymbol{\Xi}_{n+1}^{(k)}$ and $\boldsymbol{\chi}_{n+1}^{(k)}$:
$$\begin{aligned}
\boldsymbol{\Xi}_{n+1}^{(k)} &= \left[\boldsymbol{\mathcal{S}}_{n+1}^{(k)}+\partial_{\boldsymbol{\sigma}}\boldsymbol{\Lambda}_{n+1}^{(k)}(\xi_{n+1}^{(k)}-\xi_n)+\partial_{\boldsymbol{\sigma}}\mathbf{R}_{n+1}^{p(k)}\right]^{-1}\\
\boldsymbol{\chi}_{n+1}^{(k)} &= \Delta\bar{\boldsymbol{\alpha}}(T_{n+1}-T_0)+\Delta\boldsymbol{\mathcal{S}}:\boldsymbol{\sigma}_{n+1}^{(k)}+\boldsymbol{\Lambda}_{n+1}^{(k)}+\partial_{\xi}\mathbf{R}_{n+1}^{p(k)}
\end{aligned}$$
4. Calculate the increments of the martensitic volume fraction $\Delta\xi_{n+1}^{(k)}$, stress $\Delta\boldsymbol{\sigma}_{n+1}^{(k)}$, transformation strain $\Delta\boldsymbol{\varepsilon}_{n+1}^{t(k)}$ and plastic strain $\Delta\boldsymbol{\varepsilon}_{n+1}^{p(k)}$:
$$\Delta\xi_{n+1}^{(k)} = \frac{\partial_{\boldsymbol{\sigma}}\Phi_{n+1}^{(k)}:\boldsymbol{\Xi}_{n+1}^{(k)}:\left[\mathbf{R}_{n+1}^{t(k)}+\mathbf{R}_{n+1}^{p(k)}\right]-\Phi_{n+1}^{(k)}}{\partial_{\xi}\Phi_{n+1}^{(k)}-\partial_{\boldsymbol{\sigma}}\Phi_{n+1}^{(k)}:\boldsymbol{\Xi}_{n+1}^{(k)}:\boldsymbol{\chi}_{n+1}^{(k)}}$$
$$\begin{aligned}
\Delta\boldsymbol{\sigma}_{n+1}^{(k)} &= -\boldsymbol{\Xi}_{n+1}^{(k)}:\left[\mathbf{R}_{n+1}^{t(k)}+\mathbf{R}_{n+1}^{p(k)}+\boldsymbol{\chi}_{n+1}^{(k)}\Delta\xi_{n+1}^{(k)}\right]\\
\Delta\boldsymbol{\varepsilon}_{n+1}^{p(k)} &= -\mathbf{R}_{n+1}^{p(k)}-\partial_{\boldsymbol{\sigma}}\mathbf{R}_{n+1}^{p(k)}:\Delta\boldsymbol{\sigma}_{n+1}^{(k)}-\partial_{\xi}\mathbf{R}_{n+1}^{p(k)}:\Delta\xi_{n+1}^{(k)}\\
\Delta\boldsymbol{\varepsilon}_{n+1}^{t(k)} &= -\boldsymbol{\mathcal{S}}_{n+1}:\Delta\boldsymbol{\sigma}_{n+1}^{(k)}-\Delta\boldsymbol{\varepsilon}_{n+1}^{p(k)}-\left[\Delta\bar{\boldsymbol{\alpha}}(T_{n+1}-T_0)+\Delta\boldsymbol{\mathcal{S}}:\boldsymbol{\sigma}_{n+1}^{(k)}\right]\Delta\xi_{n+1}^{(k)}
\end{aligned}$$
5. Update martensitic volume fraction, transformation and plastic strains, elastic compliance tensor and thermal expansion coefficient tensor:
$$\begin{aligned}
\xi_{n+1}^{(k+1)} &= \xi_{n+1}^{(k)}+\Delta\xi_{n+1}^{(k)}\\
\boldsymbol{\varepsilon}_{n+1}^{t(k+1)} &= \boldsymbol{\varepsilon}_{n+1}^{t(k)}+\Delta\boldsymbol{\varepsilon}_{n+1}^{t(k)}\\
\boldsymbol{\varepsilon}_{n+1}^{p(k+1)} &= \boldsymbol{\varepsilon}_{n+1}^{p(k)}+\Delta\boldsymbol{\varepsilon}_{n+1}^{p(k)}\\
\boldsymbol{\mathcal{S}}_{n+1}^{(k+1)} &= \boldsymbol{\mathcal{S}}^A+\xi_{n+1}^{(k+1)}\Delta\boldsymbol{\mathcal{S}}\\
\bar{\boldsymbol{\alpha}}_{n+1}^{(k+1)} &= \bar{\boldsymbol{\alpha}}^A+\xi_{n+1}^{(k+1)}\Delta\bar{\boldsymbol{\alpha}}
\end{aligned}$$
6. Set iteration counter $k=k+1$. Go to 2.
7. Calculate consistent tangent stiffness tensor $\boldsymbol{\mathcal{L}}_{n+1}$ and thermal modulii tensor $\boldsymbol{\Theta}_{n+1}$:
$$\boldsymbol{\mathcal{L}}_{n+1} = \boldsymbol{\Xi}_{n+1}-\frac{\boldsymbol{\Xi}_{n+1}:\boldsymbol{\chi}_{n+1}\otimes\partial_{\boldsymbol{\sigma}}\Phi:\boldsymbol{\Xi}_{n+1}}{\partial_{\boldsymbol{\sigma}}\Phi:\boldsymbol{\Xi}_{n+1}:\boldsymbol{\chi}_{n+1}-\partial_{\xi}\Phi}$$
$$\boldsymbol{\Theta}_{n+1} = \boldsymbol{\Xi}_{n+1}:\left[\boldsymbol{\chi}_{n+1}\frac{\partial_{\boldsymbol{\sigma}}\Phi:\boldsymbol{\Xi}_{n+1}:\bar{\boldsymbol{\alpha}}_{n+1}-\partial_T\Phi_{n+1}}{\partial_{\boldsymbol{\sigma}}\Phi:\boldsymbol{\Xi}_{n+1}:\boldsymbol{\chi}_{n+1}-\partial_{\xi}\Phi}-\bar{\boldsymbol{\alpha}}_{n+1}\right]$$
8. Update ζ_{n+1}^d:
$$\zeta_{n+1}^d = \zeta_n^d+\frac{H_{n+1}^{\mathrm{cur}}}{H}\left|\Delta\xi_{n+1}\right|$$

4.2 Some applications of SMA constitutive models using numerical methods

In this section some applications of the numerical implementation of the SMA constitutive model, outlined in the previous section are given. Many simulations of SMA structures and devices reported in the literature (see e.g. Liang and Rogers (1990); Baz et al. (1990); Lagoudas and Tadjbakhsh (1993); Birman (1997); Panahandeh and Kasper (1997); Gillet et al. (1998)) involve strength of materials analysis of different structural SMA members (e.g. wires, rods, beams, springs), Finite Element Method (FEM) simulations of truss elements, specialized FEM beam elements, etc. These simulations deserve a separate study and will not be discussed any further here.

The potential of SMAs as load-bearing structural elements in 3-D settings was studied by Jardine et al. (1996) for torque tube actuators in aircraft wings, Liang et al. (1996) for torsional SMA actuators in helicopter rotors, Rediniotis et al. (1998) for actuation devices in underwater vehicles, Trochu and Qian (1997) for SMA spring discs and Epps and Chopra (2001) for helicopter rotor blades, among others. The need for 3-D analysis of structures with SMA actuators led to the development and integration of numerical implementations of 3-D SMA constitutive models into FEM codes.

The return mapping algorithm presented in Section 4.1, was successfully implemented in 3-D by Qidwai and Lagoudas (2000a) to solve several boundary value problems using the FEM method. Three uniaxial problems involving stress-induced pseudoelasticity, thermally induced phase transformation at constant stress, and variable stress thermally induced phase transformation were considered. Two additional 3-D problems were solved including pure torsion and combined tension-torsion of an SMA torque tube actuator. The path dependence of the state variables was investigated during the combined loading tests.

Modeling of porous SMAs has also been studied using the same numerical techniques. Qidwai et al. (2001) performed numerical simulations on a unit cell of a porous SMA matrix in order to derive overall effective thermomechanical properties. At the same time an alternative micromechanical technique based on the incremental formulation of the Mori–Tanaka method was employed and the two were compared for various loading conditions. It was found that both methods compare well in predicting the isothermal elastic material properties and pseudoelastic response under axial and out-of-plane shear loading. However, the transformation results differ under transverse and in-plane shear loading. A different approach to the same problem was taken by Entchev and Lagoudas (2002) who developed and implemented a 3-D model for porous SMAs. The porous model was derived using micromechanical averaging techniques and explicit macroscopic equations were given. A two-level numerical scheme was used to accurately predict the stress concentrations in the unit cell under different loading conditions. The model was then applied to simulate uniaxial as well as torsional and torsion-compressional loading of a porous, NiTi SMA bar.

There has also been a significant effort to simulate and predict the properties of SMA based composite materials. For example, Lagoudas et al. (1994) used an explicit return-mapping algorithm in an FEM simulation to simulate the response of an SMA fiber in a periodic unit cell. This was done as part of a larger study involving also micromechanical techniques and various fiber arrangements. Lagoudas et al. (1997) adopted the model of Boyd and Lagoudas (1996a) and further modelled the thermomechanical response of general active laminate composites with SMA strips using the layerwise finite element method. In a related work, Marfia et al. (2003) employed a different, one variant, SMA model in a layerwise beam theory to develop SMA beam finite element models. In the proposed finite element formulation the SMA material is treated as reinforcement of elastic beams. Sottos et al. (1996); Jonnalagadda et al. (1997, 1999) used FEM analysis to solve the coupled mechanical and heat conduction problem in order to analyze the transformation of embedded shape memory alloy wires and ribbons. An implicit integration was used to obtain unconditional convergence. Reisner et al. (1998) used an explicit return mapping algorithm to perform FEM simulations of Cu-Fe alloys containing very small austenitic particles dispersed in random microstructure.

Applications of SMAs involving wave propagation problems have also been considered by using the numerical implementation of the previous section (Jimenez-Victory, 1999; Lagoudas et al., 2003). Prompted by the initial analytical studies of Chen and Lagoudas (2000); Bekker et al. (2002) on simple 1-D boundary value problems in SMA rods, Jimenez-Victory (1999) used the return-mapping algorithms of Qidwai and Lagoudas (2000a) and the constitutive model of Lagoudas et al. (1996) to solve impact problems in SMA rods. Various explicit finite-difference schemes as well as the commercially available FEM solver (ABAQUS) were used. It was found that explicit, conditionally stable, finite-difference schemes were easy to implement and gave good results if sufficiently small time-steps were used. However large numerical dissipation was observed which degraded the quality of the solution with time. It was also found that standard, commercially available, semi-discrete[4] FEM solvers were not well suited for these types of highly nonlinear wave propagation problems. It should be noted that wave propagation problems involving nonlinear (hysteretic) materials present many unresolved theoretical problems (cf. eg. Renardy and Rogers (1996); Godlewski and Raviart (1996)) such as non-uniqueness of solutions and formation of shocks from arbitrarily smooth initial data, among others. While it is an open question whether traditional space-conforming, semi-discrete finite element methods are suitable for such problems, Lagoudas et al. (2003) used an adaptive finite element method along with a combined Picard-Newton iteration scheme in order to solve the wave propagation problem in SMAs. The FEM solution was compared with experimental results and the two were found to be in good agreement.

[4]that is, the spatial dimensions are discretized by conforming finite elements and the solution is marched at discrete time steps through time.

5 Conclusions

In this paper we reviewed the modeling of polycrystalline SMAs by both micromechanical approaches and phenomenological ones. A general framework of miromechanical averaging methods for polycrystalline SMAs was presented. A detailed comparison of two models published in the literature was given in order to demonstrate the micromechanical techniques used in modeling SMAs. Comparisons of simulated results with experimental observations were also summarized and found to be in good agreement for the major aspects of martensitic phase transformations: pseudoelasticity, influence of the test temperature, hysteresis loop, tension-compression asymmetry and multiaxial thermomechanical loading paths.

A broad review of phenomenological constitutive models capable of predicting the different hardening exhibited by different SMA alloys, the observed tension-compression asymmetry, detwinning, reorientation, two-way shape memory effect and transformation induced plasticity were also presented. A general thermodynamic framework was presented and was used to unify different models using the martensitic volume fraction as an internal variable. A thorough discussion of one particular SMA model capable of predicting transformation induced plasticity was also given.

The numerical integration of rate-independent SMA constitutive models and their incorporation into finite element codes was also reviewed. A typical return mapping algorithm was presented and applied to an SMA constitutive model. Finally, a brief overview of some applications of phenomenological SMA constitutive modeling in practical engineering applications was given.

Acknowledgements

The authors would like to acknowledge the support of the Air Force of Scientific Research (AFOSR), Army Research Office (ARO), the Texas Higher Education Coordinating Board, the National Air and Space Administration (NASA), and the Centre National de la Recherche Scientifique (CNRS). We would also like to express our gratitude to Bjoern Kiefer, Christophe Niclaeys, Denis Entemeyer, Parikshith Kumar, Yves Gillet, Luciano Machado, Mohammed El Amrani, Olivier Bertacchini, and Darren Hartl, who spent a significant amount of time and effort on the manuscript of this paper. E. Patoor would also like to thank Marcel Berveiller and André Eberhardt for the many fruitful discussions which led to this paper.

References

Abeyaratne, R., Kim, S.-J., 1997. Cyclic effects in shape-memory alloys: a one-dimensional continuum model. Int. J. Solids Struct. 34 (25), 3273–3289.

Abeyaratne, R., Knowles, J. K., 1994a. Dynamics of propagating phase boundaries: adiabatic theory for thermoelastic solids. Physica D 79, 269–288.

Abeyaratne, R., Knowles, J. K., 1994b. Dynamics of propagating phase boundaries: Thermoelastic solids with heat conduction. Arch. Ration. Mech. Anal. 126 (3), 203–230.

Abeyaratne, R., Knowles, J. K., 1997. Impact-induced phase transitions in thermoelastic solids. Phil. Trans. R. Soc. Lond. A 355, 843–867.

Achenbach, M., 1989. Model for an alloy with shape memory. Int. J. Plasticity 5, 371–395.

Adachi, K., Perkins, J., Wayman, C. M., 1988. The crystallography and boundary structure of interplate-group combinations of 18R martensite variant in Cu-Zn-Al shape memory alloy. Acta Metallurgica 36 (5), 1343–1364.

Anand, L., Gurtin, M., 2003. Thermal effects in the superelasticity of crystalline shape-memory materials. Journal of the Mechanics and Physics of Solids 51 (6), 1015–1058.

Argyris, J. H., Doltsinis, J. S., Knudson, W. C., Vaz, L. E., William, K. J., 1979. Numerical solution of transient nonlinear problems. Computer Methods in Applied Mechanics and Engineering 17/18, 341–409.

Auricchio, F., 2001. A robust integration-algorithm for a finite-strain shape-memory-alloy superelastic model. International Journal of Plasticity 17, 971–990.

Auricchio, F., Taylor, R. L., Lubliner, J., 1997. Shape-memory alloys: Macromodelling and numerical simulations of the superelastic behavior. Computer Methods in Applied Mechanics and Engineering 146, 281–312.

Bakhvalov, N., Panasenko, G., 1990. Homogenization: averaging processes in periodic media. Kluwer Academic Publishers, Dordrecht.

Ball, J. M., James, R. D., 1987. Fine phase mixture as minimizers of energy. Arch. Ration. Mech. Anal. 100, 13–52.

Bažant, Z. P., 1984. Microplane model for strain controlled inelastic behavior. In: Desai, C. S., Gallagher, R. H. (Eds.), Mechanics of Engineering Materials. Wiley, London, Ch. 3, pp. 45–59.

Baz, A., Iman, K., McCoy, J., 1990. The dynamics of helical shape memory actuators. J. Intell. Mater. Systems Struct. 1 (1), 105–133.

Bekker, A., Brinson, L. C., 1997. Temperature-induced phase transformation in a shape memory alloy: Phase diagram based kinetics approach. J. Mech. Phys. Solids 45 (6), 949–988.

Bekker, A., Brinson, L. C., 1998. Phase diagram based description of the hysteresis behavior of shape memory alloys. Acta Materialia 46 (10), 3649–3665.

Bekker, A., Jimenez-Victory, J. C., Popov, P., Lagoudas, D. C., 2002. Impact induced propagation of phase transformation in a shape memory alloy rod. Int. J. Plasticity 18 (11), 1447–1479.

Bensoussan, A., Lions, J., Papanicolaou, G., 1978. Assymptotic Analysis for Periodic Structures. Vol. 5 of Studies in Mathematics and its Applications. North-Holland, Amsterdam; New York; Oxford.

Berveiller, M., Morreale, J., Reubrez, E., 1994. Comportement élastoplastique des aciers lors de la mise en forme: Théorie micromécanique, simulations numériques et résultats expérimentaux. Revue Européennes des éléments finis 3 (4), 491–514.

Berveiller, M., Patoor, E., Buisson, M., 1991. Thermomechanical constitutive equations for shape memory alloys. Journal de Physique IV 1, C.4,387, European Symposium on Martensitic Transformation and Shape Memory Properties.

Birman, V., 1997. Review of mechanics of shape memory alloy structures. Appl. Mech. Rev. 50 (11), 629–645.

Bo, Z., Lagoudas, D. C., 1999a. Thermomechanical modeling of polycrystalline SMAs under cyclic loading, Part I: Theoretical derivations. Int. J. Eng. Sci. 37, 1089–1140.

Bo, Z., Lagoudas, D. C., 1999b. Thermomechanical modeling of polycrystalline SMAs under cyclic loading, Part III: Evolution of plastic strains and two-way memory effect. Int. J. Eng. Sci. 37, 1141–1173.

Bo, Z., Lagoudas, D. C., 1999c. Thermomechanical modeling of polycrystalline SMAs under cyclic loading, Part IV: Modeling of minor hysteresis loops. Int. J. Eng. Sci. 37, 1174–1204.

Bourbon, G., Lexcellent, C., Leclercq, S., 1995. Modelling of the non-isothermal cyclic behaviour of a polycrystalline Cu-Zn-Al shape memory alloy. Journal de Physique IV 5, C8–221–226.

Boyd, J. G., Lagoudas, D. C., 1994a. A constitutive model for simultaneous transformation and reorientation in shape memory materials. In: Mechanics of Phase Transformations and Shape Memory Alloys. Vol. AMD 189/PVP 292. ASME, pp. 159–172.

Boyd, J. G., Lagoudas, D. C., 1994b. Thermomechanical response of shape memory composites. J. Intell. Mater. Systems Struct. 5, 333–346.

Boyd, J. G., Lagoudas, D. C., 1996a. A thermodynamic constitutive model for the shape memory materials. Part I. The monolithic shape memory alloys. Int. J. Plasticity 12 (6), 805–842.

Boyd, J. G., Lagoudas, D. C., 1996b. A thermodynamical constitutive model for shape memory materials. Part II. The SMA composite material. Int. J. Plasticity 12 (7), 843–873.

Brinson, L. C., 1993. One-dimensional constitutive behavior of shape memory alloys: Thermomechanical derivation with non-constant material functions and redefined martensite internal variable. J. of Intell. Mater. Syst. and Struct. 4, 229–242.

Brinson, L. C., Schmidt, I., Lammering, R., 2002a. Micro and macromechanical investigations of CuAlNi single crystal and CuAlMnZn polycrystalline shape memory alloys. J. Intell. Mater. Systems Struct. 13 (12), 761–772.

Brinson, L. C., Schmidt, I., Lammering, R., 2002b. Micro and macromechanical investigations of transformation behavior of a polycrystalline NiTi shape memory alloy using in situ optical microscopy. J. Mech. Phys. Solids Submitted.

Brocca, M., Brinson, L. C., Bažant, Z. P., 2002. Three-dimensional constitutive model for shape memory alloys based on microplane model. J. Mech. Phys. Solids 50, 1051–1077.

Chen, Y.-C., Lagoudas, D. C., 2000. Impact induced phase transformation in shape memory alloys. J. Mech. Phys. Solids 48 (2), 275–300.

Christensen, R. M., 1991. Mechanics of Composite Materials. Krieger Publishing Company, Malabar, FL.

De Vos, J., Aernoudt, E., Delaey, L., 1978. The crystallography of the martensitic transformation of BCC into 9R: A generalized mathematical model. Z. Metallkde 69 (H7), 438–444.

Dederichs, P. H., Zeller, R., 1973. Variational treatment of the elastic constants of desordered materials. Z. Phys. 259, 103.

Entchev, P., 2002. Micromechanical modeling of porous shape memory alloys. Ph.D. thesis, Texas A&M University.

Entchev, P. B., Lagoudas, D. C., 2002. Modeling porous shape memory alloys using micromechanical averaging techniques. Mech. Mater. 34 (1), 1–24.

Entemeyer, D., Patoor, E., Eberhardt, A., Berveiller, M., 1995. Micromechanical modelling of the superelastic behavior of materials undergoing thermoelastic phase transition. Journal de Physique IV 5, C8–233–238.

Epps, J., Chopra, I., 2001. In-flight tracking of helicopter rotor blades using shape memory alloy actuators. Smart Mater. Struct. 10 (1), 104–111.

Falk, F., 1990. Pseudoelastic stress-strain curves of polycrystalline shape memory alloys calculated from single crystal data. Int. J. Eng. Sci. 27 (3), 277–284.

Fischer, F. D., Oberaigner, E. R., Tanaka, K., Nishimura, F., 1998. Transformation induced plasticity revised, an updated formulation. Int. J. Solids Struct. 35 (18), 2209–2227.

Gao, X., Brinson, L. C., 2002. A simplified multivariant SMA model based on invariant plane nature of martensitic transformation. J. Intell. Mater. Systems Struct. 13 (12), 795–810.

Gao, X., Huang, M., Brinson, L. C., 2000. A multivariant micromechanical model for SMAs. Part 1. Crystallographic issues for single crystal model. Int. J. Plasticity 16 (10–11), 1345–1369.

Gaymonat, G., M´uller, S., Triantafyllidis, N., 1993. Homogenization of nonlinearly elastic materials, macroscopic bifurcation and macroscopic loss of rank-one convexity. Arch. Rational Mech. Anal. 122, 231–290.

Gillet, Y., Patoor, E., Berveiller, M., 1995. Structure calculation applied to shape memory alloys. Journal de Physique IV 5, C2–343–348.

Gillet, Y., Patoor, E., Berveiller, M., 1998. Calculation of pseudoelastic elements using a non symmetrical thermomechanical transformation criterion and associated rule. Journal of Intelligent Materials and Technology 9, 366–378.

Godlewski, E., Raviart, P., 1996. Numerical Approximation of Hyperbolic Systems of Conservation Laws. No. 118 in Applied Mathematical Sciences. Springer-Verlag, New York.

Govindjee, S., Hall, G. J., 2000. A computational model for shape memory alloys. Int. J. Solids Struct. 37, 735–760.

Govindjee, S., Kasper, E. P., 1999. Computational aspects of one-dimensional shape memory alloy modeling with phase diagrams. Computer Methods in Applied Mechanics and Engineering 171, 309–326.

Govindjee, S., Miehe, C., 2001. A multi-variant martensitic phase transformation model: Formulation and numerical implementation. Computer Methods in Applied Mechanics and Engineering 191, 215–238.

Graesser, E. J., Cozzarelli, F. A., 1991. Shape memory alloys as new materials for aseismic isolation. Journal of Engineering Mechanics 117 (11), 2590–2608.

Hall, G. J., Govindjee, S., 2002. Application of a partially relaxed shape memory free energy function to estimate the phase diagram and predict global microstructure evolution. J. Mech. Phys. Solids 50, 501–530.

Hershey, A. V., 1954. The elasticity of an isotropic aggregate of anisotropic cubic crystals. J. App. Mech. 21, 236–240.

Hill, R., 1965. Continuum micromechanics of elastoplastic polycrystals. J. Mech. Phys. Solids 13, 89–101.

Hill, R., 1967. The essential structure of constitutive laws for metal composites and polycrystals. Journal of Mechanics and Physics of Solids 15, 79–95.

Huang, M., Gao, X., Brinson, L. C., 2000. A multivariant micromechanical model for SMAs. Part 2. Polycrystal model. Int. J. Plasticity 16 (10–11), 1371–1390.

Jardine, A. P., Kudva, J. M., Martin, C., Appa, K., 1996. Shape memory alloy Ti-Ni actuators for twist control of smart wing designs. In: SPIE Proceedings of Mathematics and Controls in Smart Structures. Vol. 2717. SPIE, pp. 160–165.

Jimenez-Victory, J. C., 1999. Dynamic analysis of impact induced phase transformation in shape memory alloys using numerical techniques. Master's thesis, Texas A&M University, College Station, TX 77843-3141.

Jonnalagadda, K. D., Sottos, N. R., Qidwai, M. A., Lagoudas, D. C., 1997. Transformation of embedded shape memory alloy ribbons. In: Mathematics and Controls in Smart Structures. Vol. 3039. SPIE.

Jonnalagadda, K. D., Sottos, N. R., Qidwai, M. A., Lagoudas, D. C., 1999. Transformation of embedded shape memory alloy ribbons. Journal of Intelligent Material Systems and Structures 9, 379–390.

Juhasz, L., Schnack, E., Hesebeck, O., Andra, H., 2002. Macroscopic modeling of shape memory alloys under non-proportional thermo-mechanical loadings. J. Intell. Mater. Systems Struct. 13, 825–836.

Kestin, J., Bataille, J., 1977. Continuum Models of Discrete Systems. University of Waterloo Press, Ch. Irreversible thermodynamics of continua and internal variables, pp. 39–67.

Kestin, J., Rice, J., 1970. A critical review of thermodynamics. Mono Book Corp., Baltimore, Ch. Paradoxes in the application of thermodynamics to strained solids, pp. 275–298.

Kröner, E., 1958. Berechnung der elastischen konstanten des vielkristalls aus den konstanten des einkristalls. Z. Phys. 151, 504–518.

Lagoudas, D. C., Bhattacharya, A., 1997. On the correspondence between micromechanical models for isothermal pseudoelastic responce of shape memory alloys and preisach model for hysteresis. Mathematics and Mechanics of Solids 2 (4), 405–440.

Lagoudas, D. C., Bo, Z., 1999. Thermomechanical modeling of polycrystalline SMAs under cyclic loading, Part II: Material characterization and experimental results for a stable transformation cycle. Int. J. Eng. Sci. 37, 1205–1249.

Lagoudas, D. C., Bo, Z., Qidwai, M. A., 1996. A unified thermodynamic constitutive model for SMA and finite element analysis of active metal matrix composites. Mech. Composite Mater. Struct. 3, 153–179.

Lagoudas, D. C., Boyd, J. G., Bo, Z., 1994. Micromechanics of active composites with SMA fibers. ASME Journal of Material Science and Technology 5, 337–347.

Lagoudas, D. C., Entchev, P. B., 2004. Modeling of transformation-induced plasticity and its effect on the behavior of porous shape memory alloys. Part I: Constitutive model for fully dense SMAs. Mech. Mater. 36 (9), 865–892.

Lagoudas, D. C., Moorthy, D., Qidwai, M. A., Reddy, J. N., 1997. Modeling of the thermomechanical response of active laminates with SMA strips using the layerwise finite element method. Journal of Intelligent Material Systems and Structures 8 (6), 476–488.

Lagoudas, D. C., Sarh, K., Ravi-Chandar, K., Popov, P., 2003. Dynamic loading of polycrystalline shape memory alloy rods. Mechanics of Materials 35 (7), 716.

Lagoudas, D. C., Shu, S., 1999. Residual deformations of active structures with SMA actuators. International Journal of Mechanical Sciences 41, 595619.

Lagoudas, D. C., Tadjbakhsh, I., 1993. Deformations of active flexible rods with embedded line actuators. Smart Structures and Materials 2, 72–81.

Leclercq, S., Lexcellent, C., 1996. A general macroscopic description of the thermomechanical behavior of shape memory alloys. J. Mech. Phys. Solids 44 (6), 953–980.

Lexcellent, C., Bourbon, G., 1996. Thermodynamical model for cyclic behaviour of Ti-Ni and Cu-Zn-Al shape memory alloys under isothermal undulated tensile tests. Mech. Mater. 24, 59–73.

Lexcellent, C., Leclerq, S., Gabry, B., Bourbon, G., 2000. The two way shape memory effect of shape memory alloys: an experimental study and a phenomenological model. Int. J. Plasticity 16, 1155–1168.

Lexcellent, C., Vivet, A., Bouvet, C., Calloch, S., Blanc, P., 2002. Experimental and numerical determinations of the initial surface of phase transformations under biaxial loading in some polycrystalline shape-memory alloys. J. Mech. Phys. Solids 50 (12), 2717–2735.

Liang, C., Davidson, F., Schetky, L. M., Straub, F. K., 1996. Applications of torsional shape memory alloy actuators for active rotor blade control — opportunities and limitations. In: SPIE Proceedings of Mathematics and Controls in Smart Structures. Vol. 2717. SPIE, pp. 91–100.

Liang, C., Rogers, C. A., 1990. One-dimensional thermomechanical constitutive relations for shape memory materials. Journal of Intelligent Material Systems and Structures 1, 207–234.

Liang, C., Rogers, C. A., 1992. A multi-dimensional constitutive model for shape memory alloys. Journal of Engineering Mathematics 26, 429–443.

Lim, J. T., McDowell, D. L., 1999. Mechanical behavior of a Ni-Ti shape memory alloy under axial-torsional proportional and nonproportional loading. Journal of Engineering Materials and Technology 121, 9–18.

Lipinski, P., Krier, J., Berveiller, M., 1990. Elastoplasticité des métaux en grandes déformations: Comportement global et évolution de la structure interne. Rev. Phys. Appl. 25, 361–388.

Lu, Z. K., Weng, G. J., 1998. A self-consistent model for the stress-strain behavior of shape-memory alloy polycrystal. Acta Metallurgica 46 (15), 5423–5433.

Malvern, L. E., 1969. Introduction to the Mechanics of a Continuous Medium. Prentice-Hall, Inc., Englewood Cliffs, NJ.

Manach, P. Y., 1992. Etude du comportement thermomécanique d'alliages à mémoire de forme NiTi. Ph.D. thesis, Institut National Polytechnique de Grenoble, France.

Marfia, S., Sacco, E., Reddy, J., 2003. Superelastic and shape memory effects in laminated shape-memory-alloy beams. AIAA Journal 41 (1), 100–109.

Marketz, F., Fischer, F., 1995. A mesoscale study on the thermodynamic effect of stress on martensitic transformation. Metallurgical and Materials Transactions A 26A, 267–278.

Marketz, F., Fischer, F., Tanaka, K., 1995. A computational micromechanics study on variant-coalescence in a Cu-Al-Ni shape memory alloy. Journal de Physique IV, Colloque C2 5, 537–542.

Mori, T., Tanaka, K., 1973. Average stress in matrix and average energy of materials with misfitting inclusions. Acta Metallurgica 21, 571–574.

Nemat-Nasser, S., Hori, M., 1993. Micromechanics: Overall Properties of Heterogeneous Materials. North-Holland Series in Applied Mathematics and Mechanics, vol 37. North-Holland, Amsterdam.

Ortin, J., Planes, A., 1988. Thermodynamic analysis of thermal measurements in thermoelastic martensitic transformations. Acta Metallurgica 36 (8), 1873–1889.

Ortin, J., Planes, A., 1989. Thermodynamics of thermoelastic martensitic transformations. Acta Metall. 37 (5), 1433–1441.

Ortiz, M., Pinsky, P. M., 1981. Gloabl analysis methods for the solution of elastoplastic and viscoplastic dynamic problems. Tech. Rep. UCB/SESM 81/08, Department of Civil Engineering, University of California at Berkeley.

Ortiz, M., Popov, E. P., 1985. Accuracy and stability of integration algorithms for elastoplastic constitutive relations. International Journal for Numerical Methods in Engineering 21, 1561–1576.

Ortiz, M., Simo, J. C., 1986. An analysis of a new class of integration algorithms for elastoplastic constitutive relations. Int. J. Numer. Meth. Eng. 23, 353–366.

Panahandeh, M., Kasper, E., 1997. Coupled thermomechanical simulation of shape memory alloys. In: Mathematics and Controls in Smart Structures. Vol. 3039. SPIE, pp. 468–480.

Patel, J. R., Cohen, M., 1953. Criterion for the action of applied stress in the martensitic transformation. Acta Metallurgica 1, 531–538.

Patoor, E., Bensalah, M. O., Eberhardt, A., Berveiller, M., 1992. Détermination du comportement thermomécanique des alliages à mémoire de forme par minimisation d'un potentiel thermodynamique. La Revue de Métallurgie , 1587–1592.

Patoor, E., Eberhard, A., Berveiller, M., 1988. Thermomechanical behaviour of shape memory alloys. Arch. of Mech. 40 (5-6), 775–794.

Patoor, E., Eberhardt, A., Berveiller, M., 1987. Potentiel pseudoélastique et plasticité de transformation martensitique dans les mono et polycristaux métalliques. Acta Metallurgica 35, 2779–2789.

Patoor, E., Eberhardt, A., Berveiller, M., 1994. Micromechanical modelling of the shape memory behavior. In: Brinson, L. C., Moran, B. (Eds.), Proc. ASME WAM'94: Mechanics of Phase Transformation and Shape Memory Alloys. Vol. AMD189/PVD292. ASME, pp. 23–37.

Patoor, E., Eberhardt, A., Berveiller, M., 1996. Micromechanical modelling of superelasticity in shape memory alloys. Journal de Physique IV 6, C1–277–292.

Patoor, E., El Amrani, M., Eberhardt, A., Berveiller, M., 1995. Determination of the origin for the dissymmetry observed between tensile and compression tests on shape memory alloys. Journal de Physique IV 5, C2–495–500.

Qidwai, M. A., Entchev, P. B., Lagoudas, D. C., DeGiorgi, V. G., 2001. Modeling of the thermomechanical behavior of porous shape memory alloys. Int. J. Solids Struct. 38, 8653–8671.

Qidwai, M. A., Lagoudas, D. C., 2000a. Numerical implementation of a shape memory alloy thermomechanical constitutive model using return mapping algorithms. Int. J. Numer. Meth. Eng. 47, 1123–1168.

Qidwai, M. A., Lagoudas, D. C., 2000b. On thermomechanics and transformation surfaces of polycrystalline NiTi shape memory alloy material. Int. J. Plasticity 16, 1309–1343.

Rajagopal, K. R., Srinivasa, A. R., 1998a. Mechanics of the inelastic behavior of materials. part I: theoretical underpinnigs. International Journal of Plasticity 14 (10-11), 945–967.

Rajagopal, K. R., Srinivasa, A. R., 1998b. Mechanics of the inelastic behavior of materials. part II: inelastic response. International Journal of Plasticity 14 (10-11), 969–995.

Raniecki, B., Lexcellent, C., 1994. RL-models of pseudoelasticity and their specification for some shape memory solids. Eur. J. Mech. A/Solids 13 (1), 21–50.

Raniecki, B., Lexcellent, C., 1998. Thermodynamics of isotropic pseudoelasticity in shape memory alloys. Eur. J. Mech. A/Solids 17 (2), 185–205.

Raniecki, B., Rejzner, J., Lexcellent, C., 2001. Anatomization of hysteresis loops in pure bending of ideal pseudoelastic sma beams. Int. J. Mech. Sci. 43, 1339–1368.

Rediniotis, O. K., Lagoudas, D. C., Garner, L., Wilson, N., 1998. Experiments and analysis of an active hydrofoil with sma actuators. AIAA Paper No. 98-0102, 36th AIAA Aerospace Sciences Meeting, Reno, Nevada.

Reisner, G., Werner, E. A., Fischer, F. D., 1998. Micromechanical modeling of martensitic transformation in random microstructures. Int. J. Solids Struct. 35 (19), 2457–2473.

Rejzner, J., Lexcellent, C., Raniecki, B., 2002. Pseudoelastic behavious of shape memory alloy beams under pure bending: Experiments and modelling. Int. J. Mech. Sci. 44, 665–686.

Renardy, M., Rogers, R., 1996. An Introduction to Partial Differential Equations, 2nd Edition. Texts in Applied Mathermatics. Springer-Verlag, New York.

Rice, J. R., 1971. Inelastic constitutive relation for solids: An internal variable theory and its application to metal plasticity. J. Mech. Phys. Solids 19, 433–455.

Rice, J. R., Tracey, D. M., 1973. Computational fracture mechanics. In: Fenres, S. J. (Ed.), Proceedings of the Symposium on Numerical Methods in Structural Mechanics. Academic Press, New York.

Rogueda, C., 1993. Modélisation thermodynamique du comportement pseudoélastique des alliages à mémoire de forme. Ph.D. thesis, Université de Franche-Comté, Besançon.

Roubiček, T., 2004. Models of microstructure evolution in shape memory alloys. In: Ponte Castaneda, P., Telega, J., Gambin, B. (Eds.), Nonlinear Homogenization and its Application. Vol. 170 of NATO Science Series II: Mathematics, Physics and Chemistry. pp. 269–304.

Sanchez-Palencia, E., 1980. Non-homogeneous media and vibration theory. Vol. 127 of Lecture notes in physics. Springer-Verlag, Berlin; New York.

Sato, Y., Tanaka, K., 1988. Estimation of energy dissipation in alloys due to stress-induced martensitic transformation. Res Mechanica 23, 381–392.

Shaw, J. A., 2002. A thermomechanical model for a 1-D shape memory alloy wire with propagating instabilities. Int. J. Solids Struct. 39, 1275–1305.

Shield, T. W., 1995. Orientation dependence of the pseudoelastic behavior of single crystals of Cu-Al-Ni in tension. J. Mech. Phys. Solids 43, 869–895.

Simo, J. C., Govindjee, S., 1991. Non-linear b-stability and symmetry preserving return mapping algorithms for plasticityand viscoplasticity. International Journal for Numerical Methods in Engineering , 151–176.

Simo, J. C., Hughes, T. J. R., 1998. Computational Inelasticity. Springer-Verlag New York Inc.

Simo, J. C., Ortiz, M., 1985. A unified approach to finite deformation elastoplastic analysis based on the use of hyperelastic constitutive equations. Computer Methods in Applied Mechanics and Engineering 49, 221–245.

Šittner, P., Hara, Y., Tokuda, M., 1995. Experimental study on the thermoelastic martensitic transformation in shape memory alloy polycrystal induced by combined external forces. Metallurgical and Materials Transactions A 26, 2923–2935.

Sottos, N. R., Kline, G. E., Qidwai, M. A., Lagoudas, D. C., 1996. Analysis of phase transformation fronts in embedded shape memory alloy composites. In: Mathematics and Controls in Smart Structures. Vol. 2715. SPIE, pp. 25–29.

Souza, A. C., Mamiya, E. N., Zouain, N., 1998. Three-dimensional model for solids undergoing stress-induced phase transformations. Eur. J. Mech. A/Solids 17, 789–806.

Sun, Q. P., Hwang, K. C., 1993a. Micromechanics modeling for the constitutive behavior of polycrystalline shape memory alloys — I. Derivation of general relations. J. Mech. Phys. Solids 41 (1), 1–17.

Sun, Q. P., Hwang, K. C., 1993b. Micromechanics modelling for the constitutive behavior of polycrystalline shape memory alloys — II. Study of the individual phenomena. J. Mech. Phys. Solids 41 (1), 19–33.

Sun, Q. P., Hwang, K. C., Yu, S. W., 1991. A micromechanics constitutive model of transformation plasticity with shear and dilatation effect. J. Mech. Phys. Solids 9 (4), 507–524.

Tanaka, K., 1986. A thermomechanical sketch of shape memory effect: One-dimensional tensile behavior. Res Mechanica 18, 251–263.

Tanaka, K., Hayashi, T., Itoh, Y., Tobushi, H., 1992. Analysis of thermomechanical behavior of shape memory alloys. Mechanics of Materials 13, 207–215.

Tanaka, K., Kobayashi, S., Sato, Y., 1986. Thermomechanics of transformation pseudoelasticity and shape memory effect in alloys. Int. J. Plasticity 2, 59–72.

Tanaka, K., Nishimura, F., Hayashi, T., Tobushi, H., Lexcellent, C., 1995. Phenomenological analysis on subloops and cyclic behavior in shape memory alloys under mechanical and/or thermal loads. Mechanics of Materials 19, 281–292.

Trochu, F., Qian, Y. Y., 1997. Nonlinear finite element simulation of superelastic shape memory alloy parts. Computers and Structures 67, 799–810.

Vacher, P., Lexcellent, C., 1991. Study of pseudoelastic behaviour of polycrystalline shape memory alloys by resistivity measurement and acoustic emission. In: Proc. ICM 6. Kyoto, Japan, pp. 231–236.

Wechsler, M. S., Liberman, D. S., Read, T. A., 1953. On the theory of the formation of martensite. Trans AIME 197, 1503–1515.

Wilkins, M. L., 1964. Calculation of elastic-plastic flow. In: et al., B. A. (Ed.), Methods of Computational Physics 3. Academic Press, New York.

Zaoui, A., 1985. Macroscopic plastic behaviour of microhomogeneous materials. In: Sawczuk, A., Bianchi, J. (Eds.), Plasticity Today. Elsevier, pp. 451–469.

Zhikov, V., Kozlov, S., Oleinik, O., 1994. Homogenization of Differential Operators and Integral Functionals. Springer-Verlag, Berlin; Heildelberg; New York.

Zirifi, M. E. A., 1994. Contributions à l'étude micromécanique des transformations martensitiques thermoélastiques. Ph.D. thesis, Université de Metz, France.